Memoirs of the Faculty of Engineering, Nagoya University
vol. 35, No. 2 (1983)

KINETIC STUDIES ON ION-EXCHANGE RESINS

SHIGEO GOTO and the late HIDEO TESHIMA

Department of Chemical Engineering

(Received October 25, 1983)

Abstract

Many liquid-phase reactions can be catalyzed by ion-exchange resins. Catalytic activities between ion-exchange resins and dissolved electrolytes were compared for hydrolysis of esters, such as methyl and ethyl acetates, diethyl succinate and ethyl formate. Generally, the catalytic activity of free acid was lower than that of gel-type resins while it was higher than that of macroporous type resins. The effects of mass transfer resistances on overall reaction rates and selectivities were investigated in batch reactors. As the particle sizes increased, the reaction rates and selectivities were decreased due to intraparticle diffusion resistances. Two models, that is, one realistic and one simplified, were compared with each other.

Cylindrical pellets with diameters of 3 and 5 mm were made to reduce both the pressure drop in a fixed-bed and the intraparticle diffusion resistance. The performance of reactors were studied on a recycle reactor and a tube-wall reactor. The resistances of intraparticle diffusion and interphase mass transfer in various reactors were evaluated by using ion-exchange resins.

CONTENTS

Introduction 256
1. Hydrolysis of Methyl and Ethyl Acetates in a Batch Reactor 257
  1. 1. Introduction 257
  1. 2. Experimentals 257
    1. 2. 1. Experimental method 257
    1. 2. 2. Catalysts 258
  1. 3. Theory 259
    1. 3. 1. Assumption 259
    1. 3. 2. Realistic model 259
    1. 3. 3. Simplified model 260
  1. 4. Experimental results 260

1. 4. 1. Rate constants 260
1. 4. 2. Adsorption coefficients 262
1. 5. Discussion 263
1. 5. 1. Intraparticle diffusion resistances 263
1. 5. 2. Comparison of resin catalysts with free acid catalyst 263
2. Hydrolysis of Diethyl Succinate in a Batch Reactor 264
2. 1. Introduction 264
2. 2. Experimentals 264
2. 2. 1. Experimental method 264
2. 2. 2. Catalysts 265
2. 3. Experimental results 265
2. 4. Discussion 266
2. 4. 1. Intraparticle diffusion resistances 266
2. 4. 2. Calculated concentration profiles 267
3. Oxidation of Benzyl Alcohol in a Batch Reactor 268
3. 1. Introduction 268
3. 2. Experimentals 269
3. 2. 1. Experimental method 269
3. 2. 2. Catalysts 269
3. 3. Theory 270
3. 3. 1. Reaction system 270
3. 3. 2. Adsorption system 271
3. 4. Experimental results 272
3. 4. 1. Changes in the concentrations of the reactants and products 272
3. 4. 2. Catalytic reaction 272
3. 4. 3. The effects of particle sizes on reaction rates 273
3. 4. 4. Adsorption measurements 273
3. 5. Discussion 275
3. 5. 1. Estimation of parameters from data of smaller sizes 275
3. 5. 2. Estimation of parameters from data of larger sizes 277
4. Hydrolysis of Ethyl Formate on Pellets Made of Ion-Exchange Resins in a Batch Reactor 278
4. 1. Introduction 278
4. 2. Experimentals 278
4. 2. 1. Catalysts 278
4. 2. 2. Experimental method 279
4. 3. Experimental results 280
4. 3. 1. Homogeneous reaction 280
4. 3. 2. Heterogeneous reaction 281
4. 4. Discussion 282
5. Hydrolysis of Diethyl Succinate in a Recycle Reactor 283
5. 1. Introduction 283
5. 2. Theory 283
5. 2. 1. Realistic model 283
5. 2. 2. Simplified model 285
5. 3. Experimental apparatus and procedure 285
5. 4. Results 286
5. 4. 1. Reaction rate constants from batch reactor 286
5. 4. 2. Transient responses of recycle reactor 287
5. 5. Approach time to the steady state 287
6. Hydrolysis of Ethyl Formate in a Tube-Wall Reactor 288
6. 1. Introduction 288
6. 2. Experimentals 288

6. 2. 1. Experimental method 288
6. 2. 2. Catalysts 289
6. 3. Theory 290
6. 4. Results and discussion 291
6. 4. 1. Reaction rate constant as determined in a recirculating-type of batch reactor 291
6. 4. 2. Avarage concentration at the outlet of the tube-wall catalytic reactor 292
6. 4. 3. Radial concentration distribution in the tube-wall catalytic reactor 293
7. Evaluations of Mass Transfer Resistances by Using Ion-Exchange Resins ... 294
7. 1. Evaluations of intraparticle diffusivity 294
7. 2. Simultaneous evaluations of mass transfer resistances 294
7. 3. Liquid-solid mass transfer in gas-liquid cocurrent packed beds 294
7. 4. Liquid-solid mass transfer in basket type three-phase reactors 295
Nomenclature 295
References 297

Introduction

Many chemical reactions of liquids, such as hydrolysis,[1~18] oxidation,[19~23] esterification,[24~26] alcohlysis,[27] sucrose inversion,[28, 29] aldol condensation,[30] alkylation[31] and cyanoethylation[32] can be catalyzed by ion-exchange resins.[33] Catalysis of these reactions by resins can usually be explained in terms of the catalytic activities of counter ions and is analogues to homogeneous catalysis by dissolved electrolytes.

The use of solid ion-exchange resins has the following advantages over homo geneous catalysis by dissolved electrolytes.

1) The catalyst is readily separated from the reaction products by decantation or filtration.

2) The catalyst can be re-used without regeneartion or other treatment.

3) Continuous operation in columns is possible.

4) The selectivity may be superior since side reactions are less significant.[24, 31]

5) In some cases it is possible to isolate the intermediates which cannot be obtained by homogeneous catalysis.[3]

6) Special corrosion-resistant equipment is not necessary as with some soluble catalysts.

On the other hand, the applicability of the method is restricted by the chemical and thermal stability of ion-exchange resins. Also, the resins are more expensive than dissolved electrolytes.

This report concerns the application of ion-exchange resins to the fields of chemical reaction engineering. At first, the effects of mass transfer resistances on overall reaction rates are investigated in batch reactors by using a simple reaction (Chapter 1), a complex reaction (Chapter 2), a complex reaction with two insoluble liquids (Chapter 3) and a simple reaction on cyrindrical pellets made of ion-exchange resins (Chapter 4). Then, the performances of reactors are studied on a recyle reactor with a consective reaction (Chapter 5) and a tube-wall reactor with a simple reaction (Chapter 6). Finally, the resistances of intraparticle dif-

fusion and interphase mass transfer in vorious reactors are evaluated by using ion-exchange resins (Chapter 7).

1. Hydrolysis of Methyl and Ethyl Acetates in a Batch Reactor[10~13]

1. 1. Introduction

When ion-exchange resins are used as catalysts, reactans must reach active sites in the resins and the reaction rates may be influenced by particle sizes and crosslinkings. Smith and Amundson[2] developed theoretical equations to determine the effects of intraparticle diffusion on the rates of hydrolysis of ethyl formate on Dowex 50. Saito[8] introduced the concept of effectiveness factor to analyze the overall rates.

It is important to compare catalytic activities between ion-exchange resins and dissolved electrolytes. Some investigators[1,4] found that catalytic activities of resins were higher than those of dissolved electrolytes but others[3, 5, 28, 29] reported the opposite tendency.

In this chapter, hydrolysis of methyl and ethyl acetates on two kinds of strong-acid exchange cation resins, that is, gel-type and macroprous type resins is adopted as a model of simple reaction. The effect of intraparticle diffusion is evaluated by changing the diameters of resin particles. Catalytic activities of the resins partially deactivated by sodium ion or ammonium ion are studied for comparison with those of hydrochloric acid in various concentrations.

1. 2. Experimentals

1. 2. 1. Experimental method

As shown in Fig. 1. 1, experimental apparatus consists of a reactor (1) of $1.0 \times 10^{-3} m^3$ with a condenser (2) for preventing evaporation of solution, a thermometer (3) and a motor (4) and a stirrer (5). The reactor containing $1.0 \times 10^{-3} m^3$ solution and ion-exchange resins of 20~30g was immersed into a water-bath of 40℃ and stirred at 13 rps.

An experimental run was initiated by pouring the ester into the reactor

The hydrolysis of methyl and ethyl acetates catalyzed by cation exchange resins may be represented as follows:

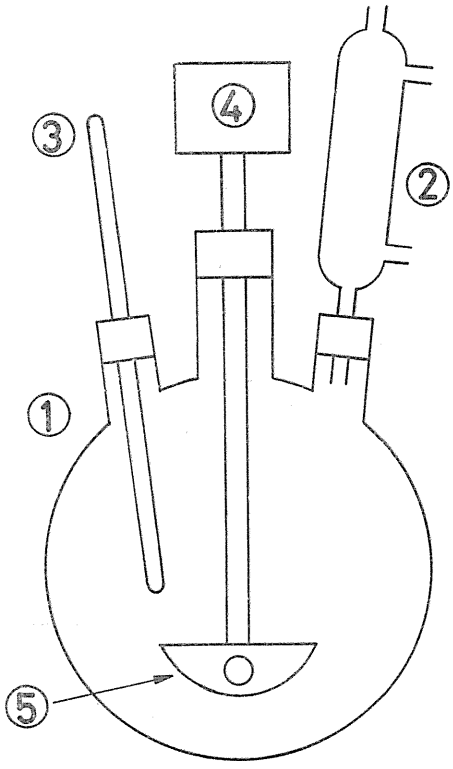

Fig. 1. 1. Experimental apparatus:
① Reactor; ② Condenser;
③ Thermometer; ④ Motor;
⑤ Impeller.

$$CH_3COOCH_3 + H_2O \longrightarrow CH_3COOH + CH_3OH \quad (1.1)$$

$$CH_3COOC_2H_5 + H_2O \longrightarrow CH_3COOH + C_2H_5OH \quad (1.2)$$

Samples were withdrawn periodically by $5.0\times10^{-6}m^3$ and titrated by 0.05 N NaOH with phenolphthalein (indicator).

Also, hydrochloric acid of 20~80mol/m^3 was used as the catalyst of free acid to compare with the catalytic activity with the resins.

1. 2. 2. Catalysts

Amberlite XE-100, IR-120B, IR-122, IR-124 were used as gel-types and Amberlyst 15 as a macroporous type. These strong acidic cation exhcange resins were treated with 1N HCl and 1N NaCl alternately two times and finally changed to H^+ form with 1 N HCl and sufficiently washed with distilled water. The swollen resins in distilled water were sieved by using JIS standard sieves. The average particle sizes (the arithmetric means of screen openings) were 0.099, 0.213, 0.460, and 0.775 mm. Crushed resins were used for less than 0.3 mm.

Table 1. 1. Characteristics of ion-exchange resins.

Resin	DVB [%]	ionic form	Q [mol/kg-dry resin]	ρ_p [kg/m^3]	ω [−]	$S_H{}^i$ [−]
Amberlite XE-100	4	H^+	5.19	1138	0.655	1
〃	4	Ha^+	0	1192	0.607	1.27
Amberlite IR-120B	8	H^+	5.07	1201	0.523	1
〃	8	Na^+	0	1275	0.475	1.44
Amberlite IR-122	10	H^+	4.97	1238	0.459	1
〃	10	Na^+	0	1317	0.404	1.56
Amberlite IR-124	12	H^+	4.73	1251	0.425	1
〃	12	Na^+	0	1323	0.391	1.65
Dowex 50W-X4	4	H^+	5.15	1130	0.671	1
Dowex 50W-X8	8	H^+	5.19	1210	0.529	1
Amberlyst 15	—	H^+	4.82	1198	0.535	1
〃	—	Na^+	0	1261	0.467	1.65
〃	—	NH_4^+	0	1196	0.518	1.94
Dowex 1X2	2	Cl^-	0	1037	0.816	—
Dowex 1X8	8	Cl^-	0	1083	0.551	—
AGMP-1	—	Cl^-	0	1069	0.594	—

The characteristics of resins are shown in Table 1. 1. DVB(%) means the percent of divinylbenzene in a resin, that is, the degree of crosslinking. The total capacity of ion-exchange resin, Q was measured by two methods. One was a batch method, that is, the resin was weighed into a flask with 1 N NaCl solution and the produced acid was titrated with 1 N NaOH solution. The other was a column method,[34] that is, a column was packed with the resin and the concentration of H^+ in the effluent was titrated with 1 N NaOH. The values of Q obtaine by two methods almost agreed each other. The density of the swollen resin, ρ_p was

measured with picnometer. The fraction of water content in the swollen resin, ω was obtained from the difference of weight between dry and swollen resins. The dry resin was weighed after drying at 105℃ in the vacuum drying oven for 2 days. The swollen resin was measured after removing adherent water by centrifugel hydroextraction at 50 rps for 10 minutes. The selectivity coefficient, $S_H{}^i$ was measured by a column method.[34]

1. 3. Theory

1. 3. 1. Assumption

The consecutive reaction represented by Eq. (1. 3) takes place on the spherical particles.

$$\mathrm{A} \longrightarrow \mathrm{R} \longrightarrow \mathrm{S} \tag{1.3}$$

The reaction rates are of first-order with respect to the amount adsorbed in the particles and are expressed by

$$\overline{R}_A = -\overline{k}_A \overline{C}_A \tag{1.4}$$

$$\overline{R}_R = \overline{k}_A \overline{C}_A - \overline{k}_R \overline{C}_R \tag{1.5}$$

$$\overline{R}_S = \overline{k}_R \overline{C}_R \tag{1.6}$$

This complex reaction can be reduced to a simple reaction by putting $\overline{k}_R = 0$.

The following assumptions are made to develop basic theoretical equations.

(1. 1) the resin-phase diffusivity is independent of position and concentration in the particles. The flux of i-component (A, R or S) can be written as

$$\overline{N}_i = -\overline{D}_i (\partial \overline{C}_i / \partial r) \tag{1.7}$$

(1. 2) Liquid film mass transfer resistance at the particle surface is negligible.

(1. 3) Adsorption equilibrium between liquid and solid is maintained at the particle surface and the linear equilibrium relation may be expressed as

$$(\overline{C}_i)_{\mathrm{sur}} = \overline{K}_i C_i \tag{1.8}$$

(1. 4) Temperature is isothermal.

(1. 5) No reactions occur in the liquid phase.

1. 3. 2. Realistic model

Mass balance equations in a batch slurry reactor are represented in the following dimentionless forms.

$$\partial z_i / \partial \theta = \delta_i \{ \partial^2 z_i / \partial \xi^2 + (2/\xi) \partial z_i / \partial \xi \} + \overline{\zeta}_i \tag{1.9}$$

Boundary conditions are

$$\mathrm{d}y_i / \partial \theta = \beta_i (\partial z_i / \partial \xi) \qquad \text{at } \xi = 1 \tag{1.10}$$

$$\partial z_i / \partial \xi = 0 \qquad \text{at } \xi = 0 \tag{1.11}$$

Initial conditions are

$$z_i=0 \qquad \text{at } \theta=0 \text{ and } 0\leq\xi\leq1 \tag{1.12}$$

$$z_i=\Phi_i(y_i)_f \qquad \text{at } \theta=0 \text{ and } \xi=1 \tag{1.13}$$

where no products are included in the feed, $(y_A)_f=1$, $(y_R)_f=0$ and $(y_S)_f=0$.

The dimensionless term, ζ_i in Eq. (1. 9) is given from Eqs. (1. 4)~(1. 6) as

$$\bar{\zeta}_A=-\alpha_A z_A \tag{1.14}$$

$$\bar{\zeta}_R=\alpha_A z_A-\alpha_R z_R \tag{1.15}$$

$$\bar{\zeta}_S=\alpha_R z_R \tag{1.16}$$

where α_i and β_i are defined as

$$\alpha_i=\bar{k}_i(d_p/2)^2/\bar{D}_A \tag{1.17}$$

$$\beta_i=3W\bar{K}_A\delta_i/(V\rho_p) \tag{1.18}$$

These equations can be solved numerically by using Saul'yev average method.[35]

1. 3. 3. Simplified model

When particles sizes are small and the reaction rates are slow, the accumulation term in Eq. (1. 9), $\partial z_i/\partial\theta$, can be neglected and the steady state approximation may be possible. Therefore, analytical solutions can be obtained as follows:

The concentration changes with time are derived as

$$y_A=\exp(-\alpha_A\beta_A E_{fA}\theta/3) \tag{1.19}$$

$$y_R=a(y^b{}_A-y_A) \tag{1.20}$$

$$y_S=1-y_A-y_R \tag{1.21}$$

where

$$a=(\delta_R-\kappa\varepsilon)/\{(\delta_R-\kappa)(1-\kappa\varepsilon\phi_R)\} \tag{1.22}$$

$$b=\kappa\varepsilon\phi_R \tag{1.23}$$

The catalytic effectiveness factor of i-componet, E_{fi}, may be given by

$$E_{fi}=(3/\sqrt{\alpha_i})(\coth\sqrt{\alpha_i}-1/\sqrt{\alpha_i}) \tag{1.24}$$

1. 4. Experimental results

1. 4. 1. Rate constants

Observed rate constants of the first order can be derived from Eq. (1. 19) for the simplified model.

$$(k_{A,v})_{\text{obs}}=\bar{K}_A\bar{k}_A E_{fA}=\rho_p V(-\ln y_A)/(Wt) \tag{1.25}$$

From experimental data of y_A vs. t in the batch reactor, the values of $(k_{A,v})_{obs}$ could be determined as a function of time. Since these values were almost independent of time, the assumption of first order was valid. Blank tests without catalyst showed that the reaction in the liquid phase was negligible. Also, negligible resistances of interphase mass transfer was confirmed by using published empirical correlation[36] of liquid-solid mass transfer coefficient.

To compare the activity of resin catalyst with free acid catalyst, the observed rate constant based on the volume of swollen resin, $(k_{A,v})_{obs}$ should be converted to that based on the equivalent of acid, $(k_{A,e})_{obs}$ as

$$(k_{A,e})_{obs}=(k_{A,v})_{obs}/Q_v \tag{1.26}$$

where the total capacity based on the swollen resin, Q_v can be defined as

$$Q_v=Q\rho_p(1-\omega) \tag{1.27}$$

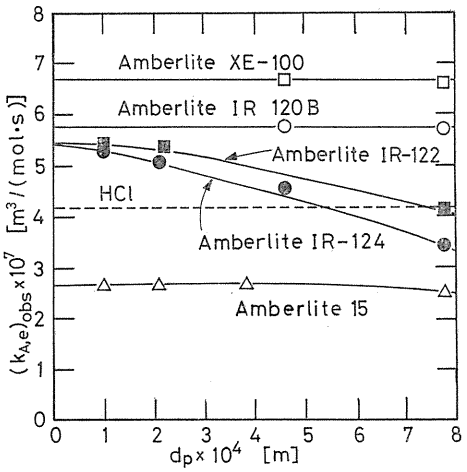

Fig. 1. 2. Effect of particle diameter on the observed rate constant for hydrolysis of ethyl acetate.

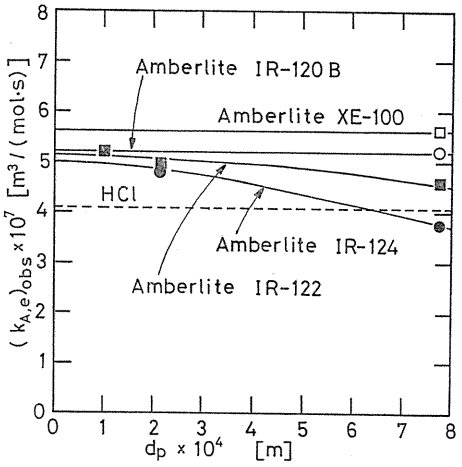

Fig. 1. 3. Effect of particle diameter on the observed rate constant for hydrolysis of methyl acetate.

Figures 1. 2 and 1. 3 show the plots of $(k_{A,e})_{osb}$ vs. particle diameters for hydrolysis of ethyl acetate and that of methyl acetate, respectively. For gel-types with higher crosslinking (Amberlite IR-122 IR-124), as the particle diameter increases, the observed rate constant is decreased due to interparticle mass transfer resistance. For gel-types with lower crosslinking (Amberlite XE-100 and IR-122B) and the macroporous type (Amberlyst 15), the intraparticle resistance is less effective and the dependence of the rate constant on particle diameters is not significant.

For the free acid catalyst, the reaction rate was almost proportional to the concentration of hydrochloric acid in the range of 50 to 1000mol/m³. Thus, the values of $(k_{A,e})_{obs}$ were independent of the concentration. The average values were shown in the dotted lines in Figs. 1. 2 and 1. 3 (4.18×10^{-7}m³/(mol·s) for ethyl acetate and 4.04×10^{-7}m³/(mol·s) for methyl acetate).

It is seen from the comparison between Figs. 1. 2 and 1. 3 that the reaction rates for ethyl acetate are higher than those for methyl acetate.

1. 4. 2. Adsorption coefficients

Flaskes which contained swollen resins in the Na^+ form and aqueous solution of the ester were immersed in the constant-temperature bath at 40℃ for 4 hours.

The adsorption coefficient of the resin in the Na^+ form, $\overline{K}_{A,Na}$ can be calculated by

$$\overline{K}_{A,\,Na}=V(C_f-C_\infty)\rho_{p,\,Na}/(W_{Na}C_\infty) \tag{1.28}$$

where $\rho_{p,\,Na}$ and W_{Na} indicate the density and the weight of the swollen resin in the Na^+ form, respectively.

For the resin in the H^+ form, direct measurements were inaccurate because the reaction took place together with the adsorption. Then, the adsorption coefficient of the resin in the H^+ form, $\overline{K}_A$ may be evaluated by using $\overline{K}_{A,\,Na}$ as follows.

$$\overline{K}_A=\overline{K}_{A,\,Na}(W_{Na}/W)(\rho_p/\rho_{p,\,Na}) \tag{1.29}$$

where ρ_p and W indicate the density and the weight of the swollen resin in the H^+ form, respectively. The value of W_{Na}/W was 0.955 for Amberlte XE-100, 0.973 for IR-122B, 0.991 for IR-122 and 0.996 for IR-124. The value of $\rho_p/\rho_{p,\,Na}$ can be calculated from Table 1. 1. The values of $\overline{K}_{A,\,Na}$ and $\overline{K}_A$ are shown in Table 1. 2.

Table 1. 2. Estimated vaules of parameters.

a) Ethyl acetate $D_{A,m}=1.45\times10^{-9}\,m^2/s$

Resin	$\overline{K}_{A,\,Na}$ [−]	$\overline{K}_A$ [−]	$(k_{A,\,e})_{int}\times10^7$ [m³/(mol·s)]	$(\overline{K}_A\overline{D}_A)\times10^{10}$ [m²/s]	$(\overline{K}_A\overline{D}_A)/D_{A,\,m}$ [−]	$\overline{D}_A\times10^{10}$ [m²/s]
Amberlite XE-100	1.35	1.23	6.68	>3.0	>0.21	>2.5
Amberlite IR-120B	1.17	1.07	5.80	>4.4	>0.31	>4.1
Amberlite IR-122	1.09	1.02	5.43	0.489	0.034	0.479
Amberlite IR-124	1.08	1.02	5.43	0.250	0.017	0.245
Amberlyst 15	0.83	0.87	2.68	>1.3	>0.09	>1.5

b) Methyl acetate $D_{A,\,m}=1.68\times10^{-9}\ m^2/s$

Resin	$\overline{K}_{A,\,Na}$ [−]	$\overline{K}_A$ [−]	$(k_{A,\,e})_{int}\times10^7$ [m³/(mol·s)]	$(\overline{K}_A\overline{D}_A)\times10^{10}$ [m²/s]	$(\overline{K}_A\overline{D}_A)/D_{A,\,m}$ [−]	$\overline{D}_A\times10^{10}$ [m²/s]
Amberlite XE-100	1.10	1.00	5.62	>2.1	>0.13	>2.1
Amberlite IR-120B	0.96	0.88	5.20	>2.5	>0.15	>2.8
Amberlite IR-122	0.90	0.83	5.25	1.349	0.080	1.61
Amberlite IR-124	0.90	0.85	5.00	0.452	0.027	0.532

1. 5. Discussion

1. 5. 1. Intraparticle diffusion resistances

The modified Thiele modulus of A-component can be defined as

$$\alpha_A E_{fA} = (d_p/6)^2 Q_v (k_{A,e})_{obs} / (\overline{K}_A \overline{D}_A) \qquad (1.30)$$

When the value of $(\overline{K}_A\overline{D}_A)$ is assumed, the effectiveness factor, E_{fA} can be calculated by the relation[37] of E_{fA} vs. $\alpha_A E_{fA}$ in Eqs. (1. 17), (1. 24) and (1. 30), and the intrinsic rate constant may be determined by $(k_{A,e})_{int} = (k_{A,e})_{obs}/E_{fA}$. If the values of $(k_{A,e})_{int}$ are independent of particle diameters, the assumed value of $(\overline{K}_A\overline{D}_A)$ becomes valid. From this procedure, the values of $(k_{A,e})_{int}$ and $(\overline{K}_A\overline{D}_A)$ for gel-types with higher crosslinking (Amberlite IR-122 and IR-124) could be estimated as indicated in Table 1. 2. The solid lines in Figs. 1. 2 and 1. 3 show the calculated values of $(k_{A,e})_{obs}$.

For gel-types with lower crosslinking (Amberlite XE-100 and IR-120B) and the macroporous type, since the resistances of intraparticle diffusion were not significant, $(\overline{K}_A\overline{D}_A)$ could not be determined. However, $(\overline{K}_A\overline{D}_A)$ might be greater than a certain value as indicated in Table 1. 2 because $E_{fA} > 0.95$ ($\alpha_A E_{fA} < 0.76$ or $\alpha_A < 0.80$).

The values of $(\overline{K}_A\overline{D}_A)/D_{A,m}$ and $\overline{D}_A$ are also indicated in Table 1. 2. The molecular diffusivity, $D_{A,m}$ was estimated by Wilke and Change's correlation.

1. 5. 2. Comparison of resin catalysts with free acid catalyst

For hydrolysis of ethyl acetate, Fig. 1. 4 shows relations of $\overline{k}_A$ vs. Q_v (or C_{HCl}) for two types of resins and hydrochloric acid. The values of Q_v could be varied by ion-exchange resins in the H^+ form partially replaced Na^+ or NH_4^+ ion.

The catalytic activity of HCl may be comparable with that of gel-types although the dependence of concentration is different. However, the activity of macroporous type is lower than that of others.

For hydrochloric acid, our data as well as previous data of Harned and Pfanstiel[38] could be correlated by

$$k_A = 4.18 \times 10^{-7} C_{HCl} \qquad (1.31)$$

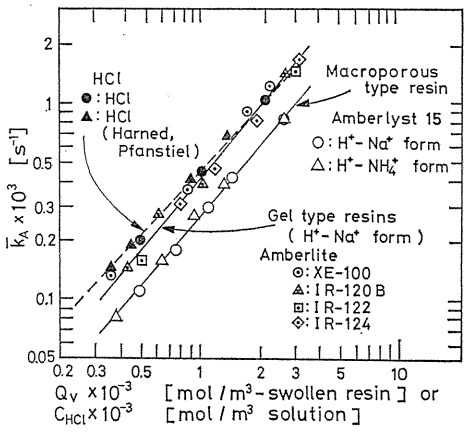

Fig. 1. 4. Catalytic activities vs. acid contents for hydrolysis of ethyl acetate.

For gel-types, the relation was independent of the degree of crosslinking and expressed by

$$\overline{k}_A = 7.20 \times 10^{-8} Q_v^{1.25} \qquad (1.32)$$

For the macroporous type, the relation was independent of the kinds of replasing ions and represented by

$$\bar{k}_A = 6.56 \times 10^{-8} Q_v^{1.20} \tag{1.33}$$

Therefore, the rate constants can be estimated from these equations.

2. Hydrolysis of Diethl Succinate in a Batch Reactor[17]

2. 1. Introduction

Many industrial reactions are encountered to complex reactions and the selectivity is an important factor as well as the catalyst activity.

In this chapter, hydrolysis of diethyl succinate catalysed by cation exchange resin of both gel and macroporous types in a batch slurry reactor is adopted as a complex reaction. Two models, that is, one realistic and one simplified, are compared with each other. The effects of crosslinking and particle size on the overall reaction rate and the selectivity are studied. Further, catalytic activities of gel and macroporous types are compared with that of free acid.

2. 2. Experimentals

2. 2. 1. Experimental method

As shown in Fig. 2. 1, experimental apparatus consists of a reactor (1) of $3.0 \times 10^{-4} m^3$ with four evenly spaced vertical buffles (2), a condenser (3) for preventing evaporation of solution, a thermometer (4) and a stirrer with 6 blades glass turbine impellers (5) and a motor (6). The reactor containing $2.9 \times 10^{-4} m^3$ solution was immersed into a water-bath at 70℃ and stirred at 10 rps.

The hydrolysis of diethyl succinate catalyzed by cation exchange resin in the H^+ form may be represented as follows:

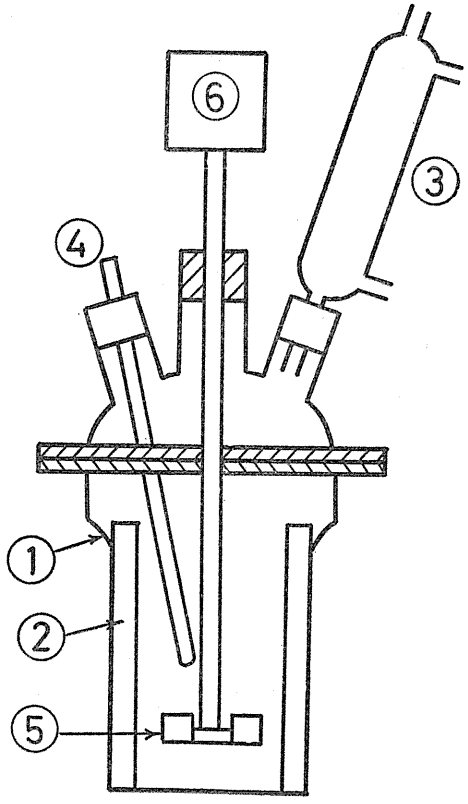

Fig. 2. 1. Experimental apparatus:
① Reactor; ② Baffle;
③ Condenser;
④ Thermometer;
⑤ Impeller; ⑥ Motor.

$$C_2H_5OCO(CH_2)_2COOC_2H_5 + H_2O \longrightarrow C_2H_5OCO(CH_2)_2COOH + C_2H_5OH \tag{2.1}$$

$$C_2H_5OCO(CH_2)_2COOH + H_2O \longrightarrow HOCO(CH_2)_2COOH + C_2H_5OH \tag{2.2}$$

An experimental run was initiated by putting the cation exchange resin into the reactor. The initial concentration of diethyl succinate was 100mol/m^3.

Samples were withdrawn every thirty minutes by micro syringe about 3.0×10^{-9}m^3 and analyzed by liquid chromatograph (Shimazu-Du pont LC-1) with the column packed with Zorbax ODS (15cm×4.6mm) at 40℃. The methanol aqueous solution of 30% was used as a mobile phase. The ultraviolet detector was set at a wavelength of 195nm. Three peaks of succinic acid, monoethyl succinate, diethyl succinate appeared in the chromatogram and these concentrations could be determined.

2. 2. 2. Catalysts

Three kinds of strong acidic cation exchange resins were used as catalysts, that is, gel-types with different crosslinkings (Dowex 50W-X4 with DVB 4% and Dowex 50W-X8 with DVB 8%) and a macroporous type (Amberlyst 15).

The characteristics of resins are shown in Table 1. 1. The swollen resin of about 10 g was weighed accurately and put into the reactor.

On the other hand, hydrochloric acid of 20~80mol/m^3 was used as the catalyst of free acid to compare with the catalytic activity with the resin in the H^+ form.

2. 3. Experimental results

Preliminary runs without catalysts indicated no changes of concentration during more than 6 hours.

For any runs with catalysts, diethyl succinate decreased with time monotonously, monoethyl succinate had a peak and succinic acid increased with time. Typical experimental results are shown in Figs. 2. 2 and 2. 3 for Dowex 50W-X8 and

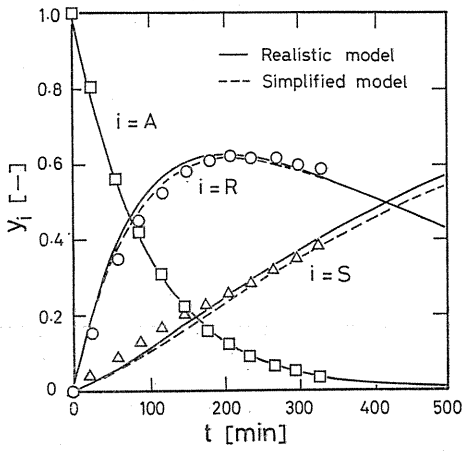

Fig. 2. 2. Comparison between experimental and calculated results for Dowex 50W-X8 at 70℃ (d_p =0.775mm, $(C_A)_f$=100mol/m^3, W=8.76g, $V=2.9\times10^{-4}$m^3, n= 8.3 rps).

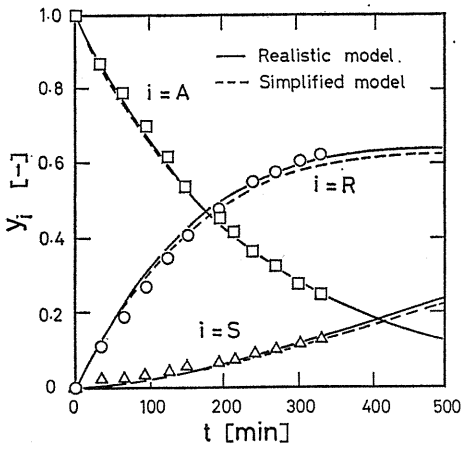

Fig. 2. 3. Comparison between experimental and calculated results for Amberlyst 15 at 70℃ (d_p =0.775mm, $(C_A)_f$=100mol/m^3, W=7.86g, V=2.9×10^{-4}m^3, n= 8.3rps).

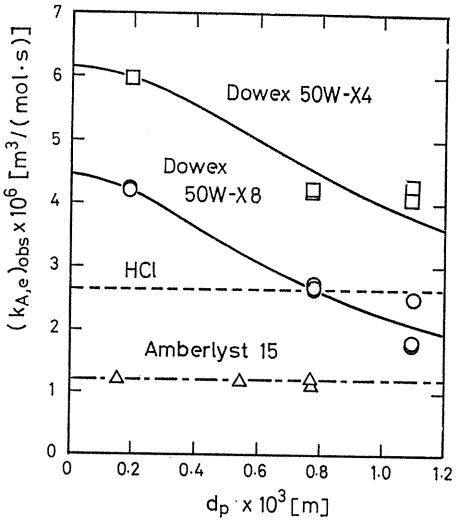

Fig. 2. 4. Effect of particle diameter on the observed rate constant.

Amberlyst 15, respectively.

When the stirring speed was changed in the range of 5 to 15 rps for the catalyst of Dowex 50X-X8, the concentrations changes with time were almost the same as those in Fig. 2. 2. Therefore, interphase mass transfer resistances could be negligible. This was confirmed by using published empirical correlation[36] of liquid-solid mass transfer coefficient.

Figure 2. 4 shows the plots of $(k_{A,e})_{obs}$ vs. d_p for various catalysts. The values of $(k_{A,e})_{obs}$ could be determined from experimental data by Eq. (1. 25). For gel-types (Dowex 50W), as the particle diameter increase, the observed reaction rate constant is decreased due to intraparticle mass transfer resistance. For the macroporous type (Amberlyst 15), the intraparticle resistance is less effective and the dependence of the rate constant on particle diameters is not significant.

For the free acid catalyst, the reaction rate was almost proportional to the concentration of hydrochloric acid in the range of 20 to 80mol/m^3. Thus, the values of $(k_{A,e})_{obs}$ were independent of the concentration. The average value was 2.63×10^{-6}m^3/(mol·s) as shown in the dotted line in Fig. 2. 4.

2. 4. Discussion

2. 4. 1. Intraparticle diffusion resistances

The intraparticle diffusion resistances can be evaluated by the same procedure as Section 1. 5. 1. The values of $(k_{A,e})_{obs}$ and $(\bar{K}_A\bar{D}_A)$ are shown in Table 2. 1.

Kataoka et al.[39] measured resin-phase diffusivities in isotopic ion-exchange and presented the estimating equation. If this equation could be applied to diethyl succinate, we might estimate $\bar{D}_A$=3.97×10^{-10}m^2/s for Dowex 50W-X4 and $\bar{D}_A$=

Table 2. 1. Estimated values of parameters.

Resin	$(k_{A,e})_{int}\times10^6$ [m³/(mol·s)]	$K_A\bar{D}_A\times10^{10}$ [m²/s]	κ [−]
Dowex 50W-X4	6.16	2.92	0.106
Dowex 50W-X8	4.45	1.50	0.103
Amberlyst 15	1.20	>5.0	0.210

2.04×10^{-10}m²/s for Dowex 50W-X8. Therefore, the adsorption equilibrium constant could be obtained from $(\bar{K}_A\bar{D}_A)$ in Table 2. 1 as $\bar{K}_A=0.74$ for both Dowex 50W-X4 and Dowex 50-X8, and thus was independent of crosslinking. On the other hand, as the crosslinking increases, the values of $\bar{D}_A$ and $(k_{A,e})_{int}$ for Dowex 50W (gel-type) are decreased.

As indicated in Table 2. 1, Amberlyst 15 (macroporous type) has a higher value of $(\bar{K}_A\bar{D}_A)$ and a lower value of $(k_{A,e})_{int}$ than Doxex-50W (gel-type). Recently, Ihm et al.[26] have proposed the model in terms of micro- and macro-effectiveness factors for Amberlyst 15. Our results may be explained by this model, that is, the micro-effectiveness factor is much less than unity but the macro-effectiveness factor is almost unity. Thus, the reaction rate is almost independent of the particle diameter but is not "true" intrinsic.

In the case of Amberlyst 15 (macroporous type) as shown in Table 2. 1, the reaction rate constant was less than hydrochloric acid and this result coincides with that of Murakami et al.[28] for sucrose inversion. On the other hand, the intrinsic reaction rate constant, $(k_{A,e})_{int}$ catalysed by Dowex 50W (gel-type) was greater than that of hydrochloric acid. The same tendencies were reported and explained by distribution factor.[8]

2. 4. 2. Calculated concentration profiles

The solid lines in Figs. 2. 2 and 2. 3 show the calculated results by using the realistic model in Section 1. 3. 2. The ratio of resin-phase diffusivity of R to A, δ_R was substituted by the ratio of molecular diffusivities in aqueous solution estimated by Wilke and Chang's equation. Estimated molecular diffusivities were $D_{A,m}=1.76\times10^{-9}$m²/s, $D_{R,m}=1.98\times10^{-9}$m²/s and $D_{R,m}/D_{A,m}=1.13$ was used as δ_R. The ratio of adsorption equilibrium constant of R to A, ϕ_R was assumed to be unity.

The ratio of reaction rate constants, κ was evaluated by using Marquart method to fit the calculated profiles of R and S-components with experimental data. The value of κ are indicated in Table 2. 1. The parameters used for the calculations are shown in foots of Figs. 1. 2 and 1. 3. The dotted lines show the profiles of the simplified model in Section 1. 3. 3. For both figures, the differences between two models are not significant. Therefore, the simplified model will be used to calculate the selectivities.

Figure 2. 5 shows the relation of y_R vs. $(1-y_A)$ for Dowex 50W-X8. The solid lines are the calculated results. Since the resistances of intraparticle diffusion are significant, the selectivity of R is decreased as the particle size increases. The results for Dowex 50W-X4 have the same tendencies. On the other hand, the

selectivities for Amberlyst 15 are independent of particle sizes because of negligible resistances as shown in Fig. 2. 6.

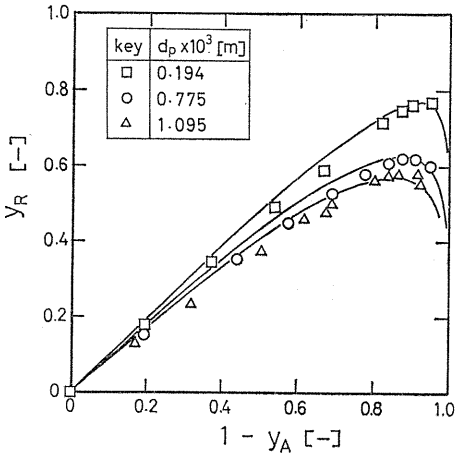

Fig. 2. 5. Effect of particle diameter on yield of *R* for Dowex 50W-X8.

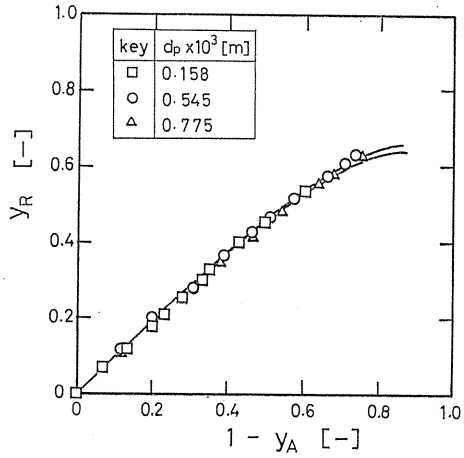

Fig. 2. 6. Effect of particle diameter on yield of *R* for Amberlyst 15.

3. Oxidation of benzyl alcohol in a batch reactor[19~23]

3. 1. Introduction

Phase transfer catalysis has been recently become of special interest to reseachers.[40]

The following reaction between two mutually insoluble substances which are dissolved in an aqueous and an organic phases, respectively takes place only at the interface.

$$RX(org)+M^{+}Nu^{-}(aq) \longrightarrow RNu(org)+M^{+}X^{-}(aq) \qquad (3.1)$$

However, if a catalyst which is soluble in the organic phase, namely a quaternary ammonium salt $Q^{+}X^{-}$, is added, the following cyclic reaction then takes place.

$$\begin{array}{lll} \text{Organic Phase} & Q^{+}Nu^{-}+RX \longrightarrow & RNu+Q^{+}X^{-} \\ \text{Interface} & \cdots\cdots\cdots\cdots \downarrow\uparrow \cdots\cdots\cdots\cdots\cdots\cdots & \downarrow\uparrow \cdots\cdots\cdots \\ \text{Aqueous phase} & Q^{+}Nu^{-}+M^{+}X^{-} \rightleftharpoons & M^{+}Nu^{-}+Q^{+}X^{-} \end{array} \qquad (3.2)$$

This is the principle of phase transfer catalysis as put by Starkes and Liotta.[40] Phase transfer catalysis is normally employed with liquid-liquid systems.

Reagan et al.[41] have made studies of the use of a solid catalyst in a liquid-liquid system. This is known as triphase catalysis, since the reaction takes place in a three-phase system (organic, solid and aqueous phases).

In this chapter, we intend to study the the reaction engineering aspects of solid phase transfer catalysis, namely the catalysis by an anion-exchange resin (solid phase) of oxidation of benzyl alcohol in toluene (organic phase) by sodium hypochlorite solution (aqueous phase). The reaction is a consecutive reaction, with benzaldehyde as the intermediate and with benzoic acid as the final product.

$$C_6H_5CH_2OH + NaClO \longrightarrow C_6H_5CHO + H_2O + NaCl \qquad (3.3)$$

$$C_6H_5CHO + NaClO \longrightarrow C_6H_5COOH + NaCl \qquad (3.4)$$

The rates of reaction and adsorption are measured in a batch reactor. Intraparticle diffusion resistances are evaluated by changing particle sizes.

3. 2. Experimentals

3. 2. 1. Experimental methods

Two types of batch reactors were used: a stirred tank and test tubes. As shown in Fig. 3. 1, the stirred tank reactor was made of glass with an internal diameter of 6. 4cm and a height of 11. 0 cm, and was fitted with four internal Teflon baffles and a six-blades turbine which was rotated at a speed of 13 rps. The test tubes were 16. 7 cm long and 2. 3 cm in internal diameter, Teflon-coated on the inside and fitted with screw caps. Mixing was achieved by vibrating the test tubes twice per second with an amplitude of 3. 5 cm. Both types of the reactors were immersed in a constant-temperature bath at 30℃.

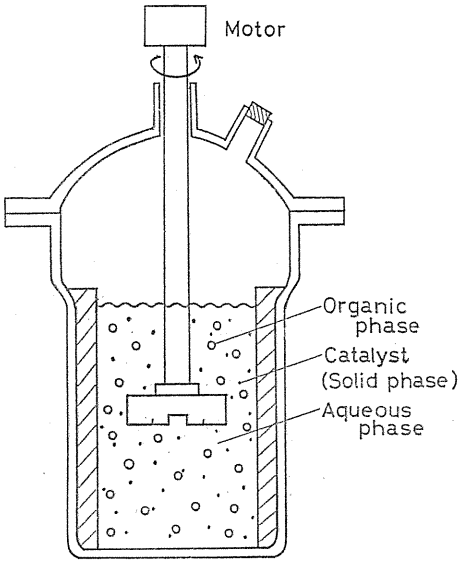

Fig. 3. 1. Batch reactor in a thermostat.

An experimental run was initiated by pouring the organic phase into the aqueous phase with resins. At predetermined intervals, the mixing was stopped to separate the organic and aqueous phases. Samples of $2.0\times10^{-9}m^3$ were then taken with a microsyringe from the upper organic phase. The sampling took less than one minute. The analysis was performed on a gas chromatograph (packing; PEG-20M, 3 m, 200℃). One mole of n-octadecane per 10 moles of benzyl alchol was added as an internal standard, and the concentrations of benzyl alchol, $C_{A,\,org}$ and benzaldehyde $C_{R,\,org}$ were determined.

In some experiments, the concentrations in the aqueous phase were determined. Samples were taken from the lower aqueous phase and were analyzed by a steam chromatograph (packing; C-1-8. 2m, 160℃).

3. 2. 2. Catalysts

Three kinds of strong anion-exchange resins were used as catalysts, that is,

gel-types with different crosslinkings (Dowex 1X2 with DVB 2% and Dowex 1X8 with DVB 8%) and a macroporous type (AGMP-1).

These resins were treated with 1 N HCl and 1N NaOH alternately two times and finally changed to Cl^- form with 1 N HCl and sufficiently washed with distilled water. Preliminary experiments showed that the catalytic activities of resins in the OH^- form were lower than those in the Cl^- form.

The characteristics of resins are shown in Table 1. 1.

3. 3. Theory

3. 3. 1. Reaction system

In a batch reactor containing three phases, the assumptions, (1. 1) ~ (1. 4) in Section 1. 3. 1 are made. However, the assumption (1. 5) is deleted and the following condition is assumed.

(3. 1) The phase equilibrium of i-component between organic and aqueous phases holds.

$$C_{i,\,\mathrm{aq}}=K_iC_{i,\,\mathrm{org}} \tag{3.5}$$

Mass balance equations in particles with initial and boundary conditions are given by

$$\partial\overline{C}_i/\partial t=\overline{D}_i\{\partial^2\overline{C}_i/\partial r^2+(2/r)\partial\overline{C}_i/\partial r\}+\overline{R}_i \tag{3.6}$$

$$\overline{C}_i=0\,;\ t=0,\quad 0<r<d_p/2 \tag{3.7}$$

$$(m_i)_f=(m_{i,\,\mathrm{org}})_f+(m_{i,\,\mathrm{aq}})_f=(m_{i,\,\mathrm{org}})_f(1+K_i\gamma)\ ;\ t=0 \tag{3.8}$$

$$\overline{C}_i=(\overline{C}_i)_f=\overline{K}_i(C_{i,\,\mathrm{org}})_f\,;\ t=0,\quad r=d_p/2 \tag{3.9}$$

$$\partial\overline{C}_i/\partial r=0\,;\ r=0,\quad t>0 \tag{3.10}$$

$$\partial m_{i,\,\mathrm{org}}/\partial t+\partial m_{i,\,\mathrm{aq}}/\partial t=-(6W/d_p)\overline{D}_i(\partial\overline{C}_i/\partial r)_{\mathrm{sur}}+R_{i,\,\mathrm{org}}V_{\mathrm{org}}+R_{i,\,\mathrm{aq}}V_{\mathrm{aq}} \tag{3.11}$$

By using dimensionless terms in Nomenclature, Eqs. (3. 6) ~ (3. 11) can be reduced to dimensionless equations as follows.

$$\partial z_i/\partial\theta=\delta_i(\partial^2z_i/\partial\xi^2+(2/\xi)\partial z_i/\partial\xi)+\overline{\zeta}_i \tag{3.12}$$

$$z_i=0\,;\ \theta=0,\quad 0<\theta<1 \tag{3.13}$$

$$z_i=(C_i)_f/(C_A)_f\,;\ \theta=0,\quad \xi=1 \tag{3.14}$$

$$\partial z_i/\partial\xi=0\,;\ \xi=0,\quad \theta>0 \tag{3.15}$$

$$\mathrm{d}y_{i,\,\mathrm{org}}/\mathrm{d}\theta=-\beta_i(\partial z_i/\partial\xi)_{\xi=1}+\zeta_{i,\,\mathrm{org}}+\zeta_{i,\,\mathrm{aq}}\ ;\ \theta>0 \tag{3.16}$$

where

$$\beta_i=3\overline{\gamma}\overline{K}_A\delta_i/\{(1+\gamma K_A)(1+\gamma K_i)\} \tag{3.17}$$

$$\overline{\zeta}_i=\mathrm{d}_p{}^2\overline{R}_i/\{4\overline{D}_A(\overline{C}_A)_f\} \tag{3.18}$$

$$\zeta_{i,j}=\gamma d_p^2 R_{i,j}/\{4\overline{D}_A(1+\gamma K_i)(C_A)_f\}\ ;\ j=\text{org or aq} \tag{3.19}$$

The consecutive reaction represented by Eq. (1. 3) takes place in both organic and aqueous phases as well as on the resin phase.

The reaction rates of first order in the liquid phase (j=org or aq) are expressed by

$$R_{A,j}=-k_{A,j}C_{A,j} \tag{3.20}$$

$$R_{R,j}=k_{A,j}C_{A,j}-k_{R,j}C_{R,j} \tag{3.21}$$

Equations (3. 20) and (3. 21) can be reduced to the following equations by using Eq. (3. 19).

$$\zeta_{A,j}=-\alpha_{A,j}y_{A,j} \tag{3.22}$$

$$\zeta_{R,j}=\alpha_{A,j}y_{A,j}-\alpha_{R,j}y_{R,j} \tag{3.23}$$

The reaction rates on the resin phase can be expressed by Eqs. (1. 4) and (1. 5) and the dimensionless terms, $\bar{\zeta}_A$ and $\bar{\zeta}_R$ by Eqs. (1. 14) and (1. 15).

These equations can be solved numerically by using the Saul'yev average method[35] to obtain the relations of $y_{i,\text{org}}$ and t.

When the intraparticle diffusion resistances are negligible, the first term in the right side of Eq. (3. 11) should be changed to $\overline{R}_i W/\rho_p - d\overline{m}_i/dt$. Analytical solutions can be obtained as follows.

$$y_{A,\text{org}}=\{\exp(-b_A t/a_A)\}/a_A \tag{3.24}$$

$$y_{R,\text{org}}=b_A\{\exp(-b_A t/a_A)-\exp(-b_R t/a_R)\}/(a_A b_R-a_R b_A) \tag{3.25}$$

Where ($i=A$ or R)

$$a_i=1+\gamma K_i+\bar{\gamma}\overline{K}_i \tag{3.26}$$

$$b_i=k_{i,\text{org}}+\gamma k_{i,\text{aq}}K_i+\bar{\gamma}\bar{k}_i\overline{K}_i \tag{3.27}$$

3. 3. 2. Adsorption system

Mass balance equations can be obtained by deleting the terms of reaction rates in Eqs. (3. 6) and (3. 11).

For the linear isotherm expressed by Eq. (1. 8), analytical solution can be obtained.[42]

$$\begin{aligned} E&=\{(C_{i,\text{org}})_f-C_{i,\text{org}}\}/\{(C_{i,\text{org}})_f-(C_{i,\text{org}})_\infty\} \\ &=1-(2/3e)\exp(-s_n^2\delta_i\theta)/\{1+s_n^2/(9e+e^2)\} \end{aligned} \tag{3.28}$$

where s_n is the n-th positive root of the following equation.

$$s_n\cot s_n=1+s_n^2/(3e) \tag{3.29}$$

$$e=\{1-(C_{i,\text{org}})_\infty/(C_{i,\text{org}})_f\}/\{(C_{i,\text{org}})_\infty/(C_{i,\text{org}})_f\} \tag{3.30}$$

3. 4. *Experimental results*

3. 4. 1. *Changes in the concentrations of the reactants and products*

In order to elucidate the reaction mechanism, measurements were made over a long period of time as shown in Fig. 3. 2 for Dowex 1X2. The benzyl alchol concentrations in both the organic and aqueous phases decreased monotonously, with the ratio $K_A = C_{A,\,aq}/C_{A,\,org}$ being nerly constant and being always distribution equlibruim. The benzylaldehyde concentration increased with time, and then decreased after passing a maximum, thus showing the reaction was a consecutive reaction. Since the solubility of bezylaldehyde in the aqueous phase was low, there were appreciable errors in the measurements. The presence of final product, benzonic acid, was detected on the steam chromatograph but its concentration could not be quantitatively determined owing to interference by the sodium hypochlorite.

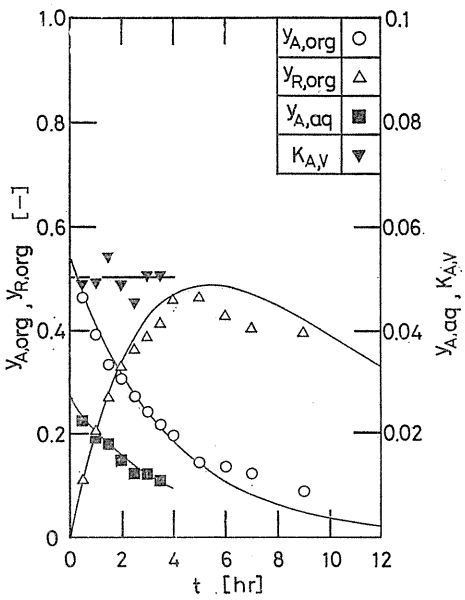

Fig. 3. 2. Variations of concentrations with time ($\gamma=5$, $\bar{\gamma}=0.386$, $(C_A)_f=193$ mol/m^3).

3. 4. 2. *Catalytic reaction*

By fixing the ratio of the aqueous and organic phases constant at $\gamma=5.0$ and the initial benzyl alcohol concentration, $(C_A)_f$ constant at 193mol/m^3, reactions were carried out by changing resin concentrations, $\bar{\gamma}$ and benzyl alcohol and benzylaldehyde concentrations in the organic phase were measured. The results are shown in Fig. 3. 3 for Dowex 1X2. An increase in the resin concentration increased the reaction rate, thus confirming the catalytic activity of this resin. As $\bar{\gamma}$ was increased, there was overall decrease in the value of $y_{A,\,org}$, which was due to the adsortion of the benzyl alcohol on the catalyst. Even at $\bar{\gamma}=0$, the reaction still proceeded to some extent.

Figure 3. 4 shows the effect of ratio γ of the volumes of the aqueous and organic phases on the reaction in the absence of an ion-exchange resin ($\bar{\gamma}=0$). A higher value of γ, that is, the more aqueous phase present, favored the reaction. When $y_{A,\,org}$ was extrapolated to $t=0$, the values of $y_{A,\,org}$ were not unity because benzyl alcohol was distributed into the aqueous phase.

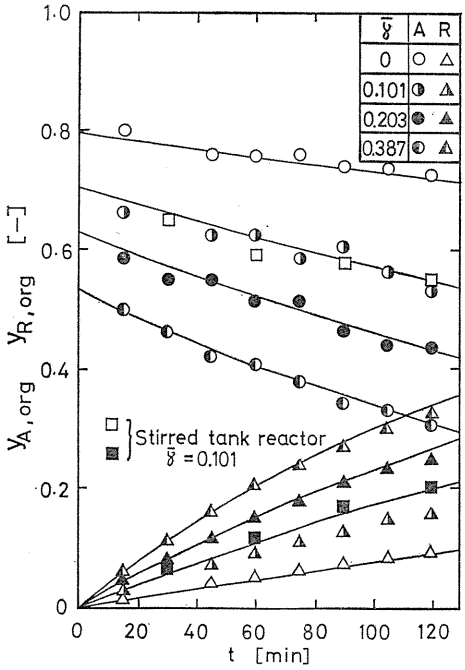

Fig. 3. 3. Effect of concentration of catalyst on reaction rate (γ=5, $(C_A)_f$=103mol/m^3).

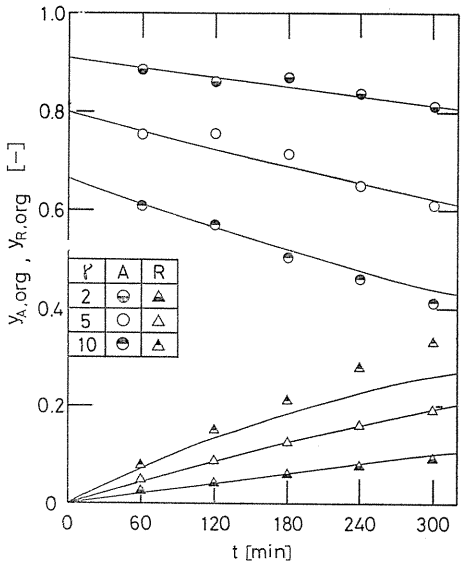

Fig. 3. 4. Effect of γ on reaction rate ($\bar{\gamma}$=0, $(C_A)_f$=580mol/m^3).

3. 4. 3. The effects of particle sizes on reaction rates

Measurements for Dowex 1X8 and AGMP-1 were made by changing the particle diameter, d_p from 0.056 to 0.795 cm while fixing $(C_A)_f$=193mol/m^3, γ=5.0 and $\bar{\gamma}$=0.093. Figure 3. 5 shows the results for smaller sizes of Dowex 1X8 (d_p=0.056 and 0.112cm). Since there were no differences of results between 0.056 and 0.112 cm, intraparticle diffusion resistances were negligible in these regions. The results for larger sizes (0.400 and 0.795cm) are shown in Fig. 3. 6. As the diameter increased, the reaction rate was decreased and then intraparticle diffusion resistances became significant.

Figure 3. 7 shows the results of two extreme sizes for AGMP-1 (0.056 and 0.795cm).

3. 4. 4. Adsorption measurements

Measurements were made of the amount of benzyl alcohol and benzaldehyde adsorbed on the ion-exchange resin, with distilled water being used as the aqueous phase in place of aqueous sodium hypochlorite, so that no reaction would take place. The resulting isotherms are shown in Fig. 3. 8 for Dowex 1X2. The graphs of $C_{A,org}$ vs. $\bar{C}_A$ and $C_{R,org}$ vs. $\bar{C}_R$ were approximated by straight lines through the origin. From the slopes, we have $\bar{K}_A$=1.60 and $\bar{K}_R$=0.111.

The adsorption of benzadehyde was less than that of benzyl alcohol by a factor of about 14. The value of γ had no effect on the adsorption, which shows that

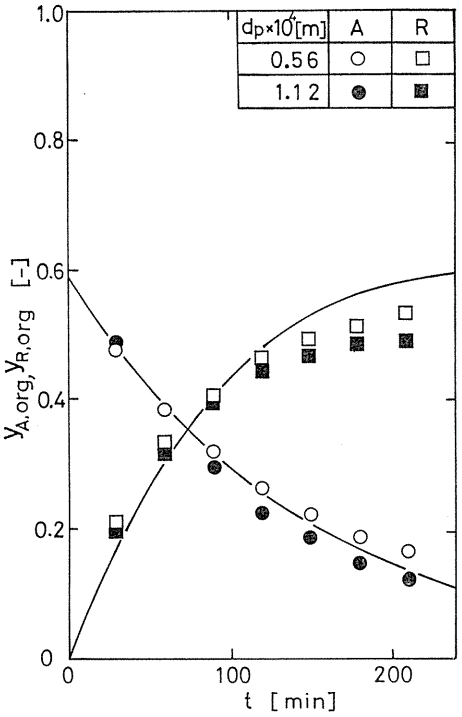

Fig. 3. 5. $y_{A,\,org}$, $y_{R,\,org}$ vs. t for Dowex 1X8 (d_p=0.056 and 0.112mm, γ=5, $\bar{\gamma}$=0.093, $(C_A)_f$=193mol/m³).

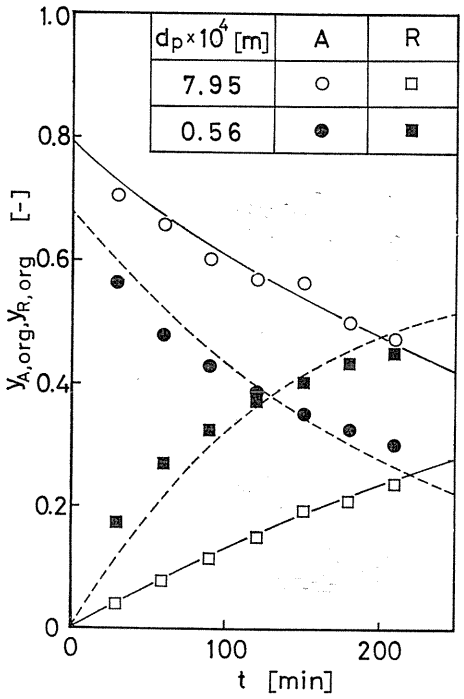

Fig. 3. 7. $y_{A,\,org}$, $y_{R,\,org}$ vs. t for AGMP-1 (d_p=0.056 and 0.795mm, γ=5, $\bar{\gamma}$=0.093, $(C_A)_f$=193mol/m³).

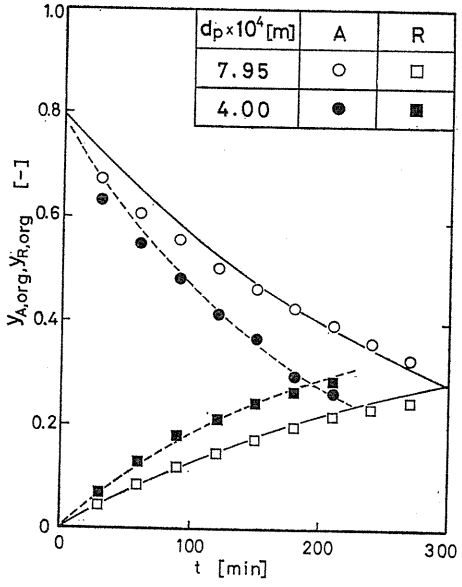

Fig. 3. 6. $y_{A,\,org}$, $y_{R,\,org}$ vs. t for Dowex 1X8 (d_p=0.40 and 0.795mm, γ=5, $\bar{\gamma}$=0.093, $(C_A)_f$=193mol/m³).

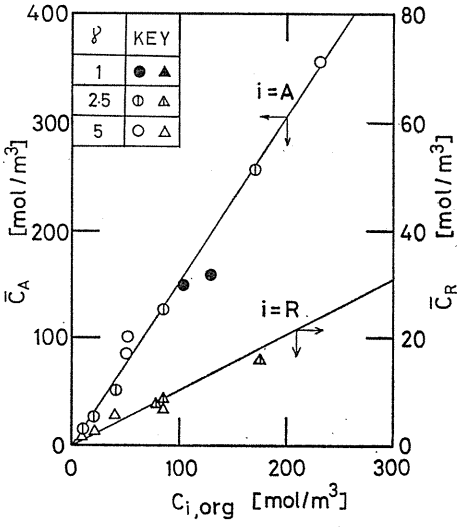

Fig. 3. 8. Adsorption isotherms at 30℃ for Dowex 1X2.

there was an adsorption equilibrium between benzyl alcohol (benzaldehyde) in the organic phase and that on the resin phase.

The rates of adsorption were measured by changing $(C_A)_f$, γ and $\bar{\gamma}$ as indicated in Table 3. 1. The results show in Figs. 3. 9 and 3. 10 for Dowex 1X8 and AGMP-1, respectively. The solid lines indicate results calculated form Eq. (3. 28) by adjusting $\bar{D}_A$ as shown in Table 3. 1.

Table 3. 1. The value of $\bar{D}_A$ obtained from adsorption measurements. (d_p=7.95×10^{-4}m)

Run No.	$(C_A)_f$ [mol/m^3]	γ [−]	$\bar{\gamma}$ [−]	Dowex 1X8		AGMP-1	
				$\bar{K}_A$ [−]	$\bar{D}_A\times10^{11}$ [m^2/s]	$\bar{K}_A$ [−]	$\bar{D}_A\times10^{11}$ [m^2/s]
A-1	180	5	0.102	0.408	1.33	0.413	2.79
A-2	180	2	0.093	0.381	1.25	0.386	2.40
A-3	180	1	0.093	0.377	1.90	0.368	3.65
A-4	180	0	0.130	—	1.68	—	3.70
A-5	90	5	0.112	0.401	1.05	0.424	3.08
A-6	360	5	0.102	0.389	1.31	0.366	3.28
			Average		1.42		3.15

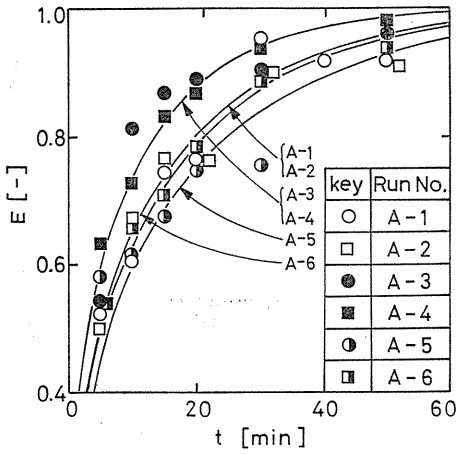

Fig. 3. 9. E vs. t for Dowex 1X8.

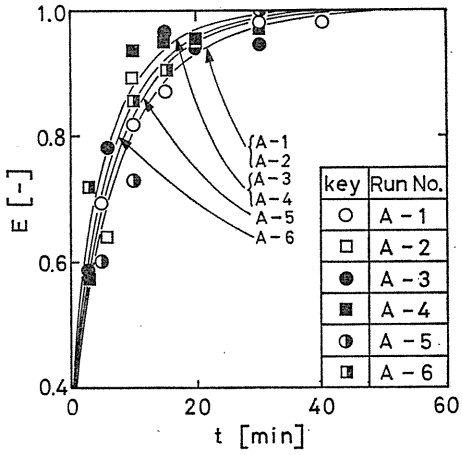

Fig. 3. 10. E vs. t for AGMP-1.

3. 5. Discussion

3. 5. 1. Estimation of parameters from data of smaller sizes

For negligible resistances of intraparticle diffusion, Eq. (3. 24) can be rearranged as

$$-\ln y_{A,\,\mathrm{org}}=\ln a_A+(b_A/a_A)t \tag{3. 31}$$

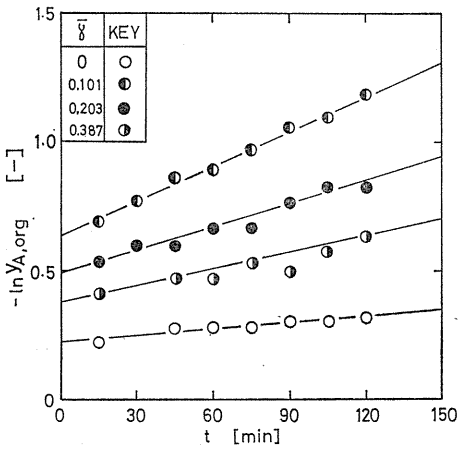

Fig. 3. 11. $(-\ln y_{A,\mathrm{org}})$ vs. t ($\gamma=5$, $(C_A)_f=193\mathrm{mol/m^3}$).

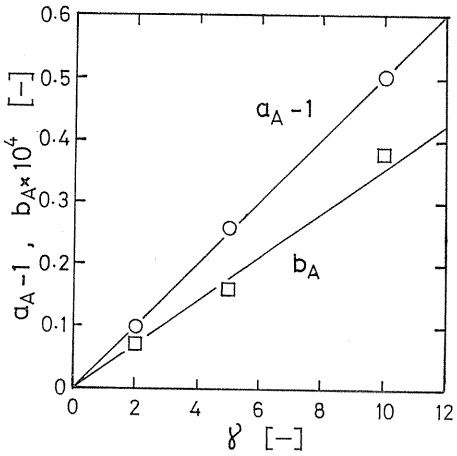

Fig. 3. 12. (a_A-1) and b_A vs. γ at $\bar{\gamma}=0$.

Figure 3. 11 shows a plot of our experimental data in Fig. 3. 3 in the form of a graph of $(-\ln y_{A,\mathrm{org}})$ vs. t. Since lines are approximately straight, the assumption of first forder with respect to benzyl alcohol became valid. The intercept represents a_A and the slope b_A. The similar results for benzaldehyde were obtained.

Figure 3. 12 shows the relation of (a_A-1) and b_A vs. γ in the absence of a catalyst ($\bar{\gamma}=0$). This graph was constructed by replotting data in Fig. 3. 4 in the form of $(-\ln y_{A,\mathrm{org}})$ vs. t and then reading off the intercepts and slopes of the straight lines. If the substitutions i=A and $\bar{\gamma}=0$ in Eqs. (3. 26) and (3. 27) are made, we have

$$a_A-1=\gamma K_A \tag{3. 32}$$

$$b_A=k_{A,\mathrm{org}}+\gamma k_{A,\mathrm{aqg}}K_A \tag{3. 33}$$

The graph of (a_A-1) vs. γ in Fig. 3. 12 is a straight line through the origin, which confirms that the benzyl alcohol was in phase equilibrium, and from the slope we obtain $K_A=0.0504$. The graph of b_A vs. γ was also approximated by a straight line through the origin, and from the intercept and the slope we obtain $k_{A,\mathrm{org}}=0$ and $k_{A,\mathrm{aq}}=6.93\times10^{-5}\mathrm{s}^{-1}$. The fact that $k_{A,\mathrm{org}}=0$ means that the reaction did not proceed in the organic phase.

Figure 3. 13 shows the relationship of (a_A-1) and b_A vs. γ based on data in Fig. 3. 11. By putting i=A in Eqs. (3. 26) and (3. 27), we have

$$a_A-1=\gamma K_A+\bar{\gamma}\bar{K}_A \tag{3. 34}$$

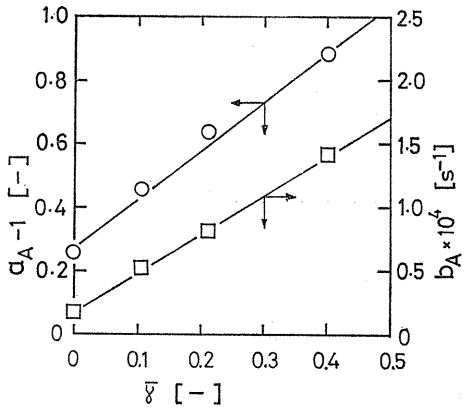

Fig. 3. 13. (a_A-1) and b_A vs. $\bar{\gamma}$ at $\gamma=5$.

$$b_A = k_{A,\,org} + \gamma k_{A,\,aqg} K_A + \bar{\gamma} \bar{k}_A \bar{K}_A \tag{3.35}$$

Thus, from the slope of the linear graphs in Fig. 3. 13, we obtain $\bar{K}_A = 1.59$ and $\bar{k}_A = 2.00 \times 10^{-4} s^{-1}$.

Table 3. 2 lists the estimated values of the parameters obtained in this way. The solid lines in Figs. 3. 2~3. 5 and 3. 7 represent calculated results obtained by substituting these values into Eqs. (3. 24) and (3. 25), there being close agreement with the empirical results. The figures in parentheses of Table 3. 2 represent the adsorption equilibrium constants obtained in the adsorption experiments, which agreed with those of the reaction system.

Table 3. 2. Estimated values of constants.

Catalyst	$\bar{K}_A$ [−]	$\bar{k}_A \times 10^4$ [s^{-1}]	$\bar{K}_R$ [−]	$\bar{k}_R \times 10^3$ [s^{-1}]	$\bar{D}_A \times 10^{13}$ [m^2/s]
Dowex 1X2	1.59(1.60)[a]	2.00	0.107(0.111)[a]	0.586	—
Dowex 1X8	4.59	4.15	0.0824	2.52	9.00
AGMP-1	2.19	4.50	0.236	0.674	15.0

a) Adsorption experiments

$K_A = 5.04 \times 10^{-2}$ $K_R = 4.86 \times 10^{-3}$
$k_{A,\,aq} = 6.93 \times 10^{-5} s^{-1}$ $k_{R,\,aq} = 5.10 \times 10^{-4} s^{-1}$
$k_{A,\,org} = 0 s^{-1}$ $k_{R,\,org} = 0 s^{-1}$

3. 5. 2. Estimation of parameters from data of larger sizes

For significant resistances of intraparticle diffusion, Eqs. (3. 12) ~ (3. 23) were solved numerically. The optimal values of $\bar{D}_A$ could be determined by curve fitting to observed values in Figs. 3. 6 and 3. 7. As shown in Table 3. 2, $\bar{D}_A$ for the macroporous type, AGMP-1 is larger by 1. 7 times than that for gel-type, Dowex 1X8. From the comparison between Tables 3. 1 and 3. 2 the values of $\bar{D}_A$ in the reaction system were much lower than those in the adsorption system. The values of $\bar{D}_R$ were calculated from the assumption of $\delta_R = \bar{D}_R / \bar{D}_A = D_{R,m} / D_{A,m} = 1.06$. Molecular diffusivities of A and R were estimated from Wilke and Chang's equation.

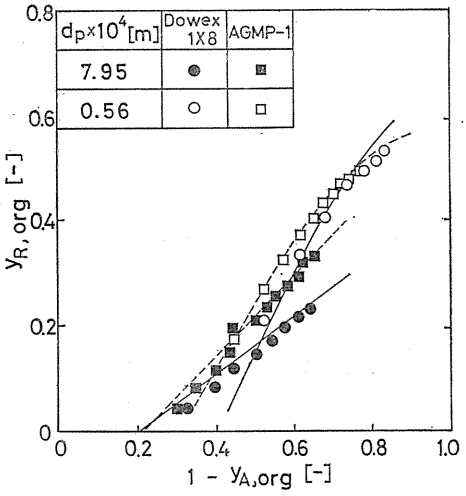

Fig. 3. 14. $y_{R,\,org}$ vs. $(1 - y_{A,\,org})$.

Figure 3. 14 shows the relation of $y_{R,\,org}$ vs. $(1 - y_{A,\,org})$ for two extreme sizes ($d_p = 0.056$ and 0. 795mm). Solid and dotted lines are calculated results for Dowex 1X8 and AGMP-1, respectively. Since the resistances of intraparticle diffusion are significant, the selectivity of R is decreased as the particle size increases.

4. Hydrolysis of Ethyl Formate on Pellets Made of Ion-Exchange Resins in a Batch Reactor[18]

4. 1. Introduction

Since the diameter of conventional ion-exchang resin particles are less than 1 mm, the pressure drops may be very high in fixed-bed reactors packed with the resin particles. On the hand, as the particle sizes increased, the intraparticle diffusion resistances are increased.

In this chapter, cylindrical pollets with diameters of 3~5 mm were made to solve this contradiction. Hydrolysis of ethyl formate takes place in batch reactors to compare catalytic activities of these resin pellets with those of resin particles.

$$HCOOC_2H_5+H_2O \longrightarrow HCOOH+C_2H_5OH \qquad (4.1)$$

4. 2. Experimentals

4. 2. 1. Catalysts

The cation-exchange resin of macroporous type, Amberlyst 15 was used. The average diameters of swollen resins, d_p were 0.53 and 0.75mm for spherical particles and 0.095mm for crushed particles.

Cylindrical pellets with 3×3 mm and 5×5 mm were made by mixing these resin particles with 15 wt% binding powder (polyethylene, less than 0.15mm) and heated to 140℃ in moulds for one hour.

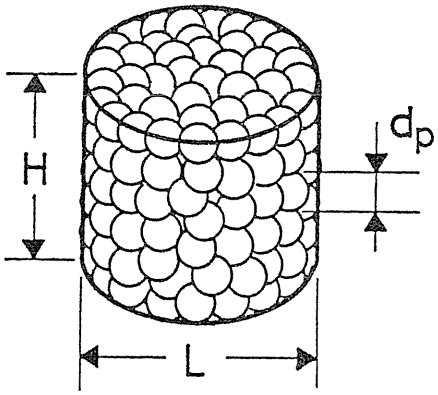

Fig. 4. 1. (a) Pellet made of spherical resin particles.

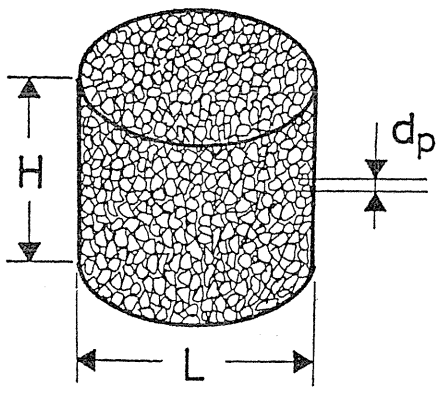

Fig. 4. 1. (b) Pellet made of crushed resin particles.

Systematic drawings of pellets made of spherical particles and crushed particles are shown in Figs. 4. 1 (a) and (b), respectively. The characteristics of Amberlyst 15 for particles and pellets are shown in Table 1. 1 and 4. 1. The values of L and H in parentheses indicate the diameters and heights of pellets at dry resins. The equivalent diameter D_p, was calculated by $D_p=(3L^2H/2)^{1/3}$. The void fraction of pellet, ε_p' may be defined as $(1-\rho_{pellet}/\rho_{particle})$. As the particle diameter decreased, the density of pellet, ρ_{pellet}, was increased and then the value of ε_p' became

smaller.

Table 4. 1. Characteristics of cylindrical pellets. (Amberlyst 15)

Resin	$d_p \times 10^3$ [m]	$L \times 10^3$ [m]	$H \times 10^3$ [m]	$D_p \times 10^3$ [m]	ρ_{pellet} [kg/m³]	ε'_p [−]	Q [mol/kg-dry resin]	ω [−]
Pellet (1)	0.75	5.8(5.0) 3.4(3.0)	5.0(4.3) 3.5(3.1)	6.3 4.0	763	0.360	4.05	0.489
Pellet (2)	0.53	5.8(5.0) 3.4(3.0)	4.6(4.0) 3.8(3.4)	6.1 4.1	834	0.300	3.98	0.492
Pellet (3)	0.095	5.7(5.0) 3.3(3.0)	4.0(3.5) 2.8(2.5)	5.8 3.6	846	0.290	3.30	0.452

4. 2. 2. Experimental method

The stirred tank reactor containing $1.0 \times 10^{-3} m^3$ solution as shown in Fig. 4. 2 (a) was used for resin particles. The rotating catalytic basket reactor (the inner

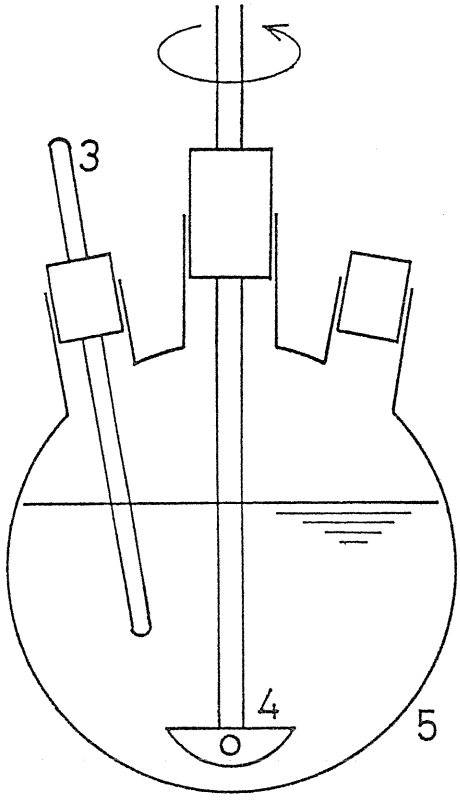

Fig. 4. 2. (a) Stirred slurry reactor.

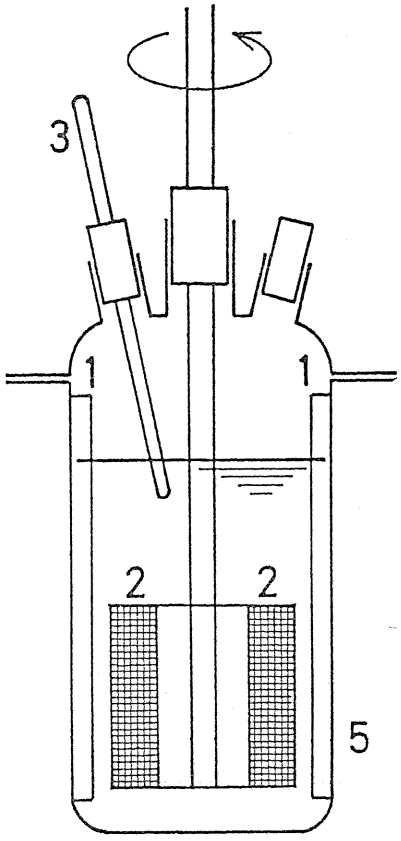

Fig. 4. 2. (b) Rotating catalytic basket reactor:

① Baffle; ② Catalytic basket; ③ Thermometer; ④ Impeller; ⑤ Vessel.

diameter = 8.2cm, the height = 19.5cm) in Fig. 4. 2(b) was used for resin pellets to prevent the sedimentation of catalysts into the bottom. Two catalytic baskets with stainless steel screens were attached to the axis of the stirrer. These reactors were immersed into a water-bath of 30, 40 or 50℃.

An experimental run was initiated by pouring ethyl formate into the reactor.

The sample which was taken from the reactor was quickly introduced into a triangular flask containing $5.0\times10^{-5}m^3$ of distilled water, which had been precooled to around 0℃ by immersed in iced water containing salt. The contents of the flask were titrated against a 0.1 N aqueous solution of NaOH using phenolphtalein as the indicator, and the concentration of formic acid which was formed was calculated. The cooling procedure was designed to limit as much as possible any saponification of the ethyl formate during the course of the neutralization titration.

The total concentration of ethyl formate and formic acid, C_t was determined in the following way. 0.1 N NaOH solution was added to a sample of the liquid in the feed reservoir and the mixture was stirred well and then back-titrated against 0.1 N HCl using phenolphtalein as the indicater, and the total concentration was calculated from the amount of NaOH which had been consumed in the saponification.

4. 3. Expermiental results

4. 3. 1. Homogeneous reaction

The rate of homogeneous reaction is assumed to be proportional to both concentrations of ethyl formate and hydrogen ion.[43] The hydrogen ion may be produced by the dissociation of the product, formic acid. Since formic acid is a weak acid, the concentration of hydrogen ion may be proportional to the root of the concentration of formic acid.

$$-dC_A/dt=k_HC_HC_A=k_H\sqrt{K_HC_R}\cdot C_A \qquad (4.2)$$

where the dissociation constant, K_H may be $0.176mol/m^3$ in this experimental conditions. Since water was present in excess to ethyl formate, the backward reaction might be negligible.

Figure 4. 3 shows the unconversions, $(1-X_A)$ vs. t for various values of initial mole fractions of formic acid, $y_{R,0}$ and reaction temperatures, T.

By integrating Eq. (4. 2), we have

$$k_H=(1/t_i\sqrt{K_H})\int_0^{X_{A,i}} dX_A/[(1-X_A)\sqrt{\{(1-y_{R,0})X_A+y_{R,0}\}C_t}] \qquad (4.3)$$

where $X_{A,i}$ indicates the conversion of formic acid at the period from t_{i-1} to t_i.

The values of k_H could be determined from data of Fig. 4. 3. The dotted line in Fig. 4. 4 shows Arrhenius plot of k_H. From the slope, the activation energy was 62.4kJ/mol, which was in an agreement with that of 61.4kJ/mol for HCl catalyst.[43]

The solid and dotted lines in Fig. 4. 3 are the calculated values from Eq. (4. 2).

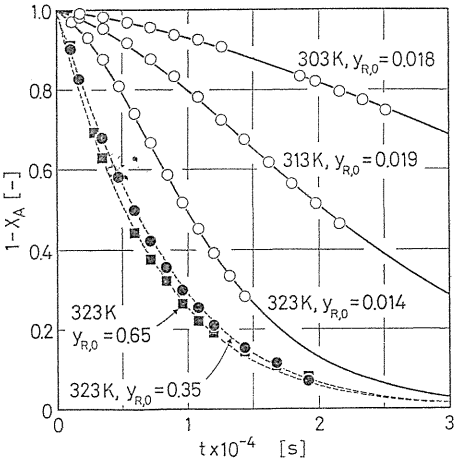

Fig. 4. 3. Conversion changes with time for the homogeneous reaction (C_t=321mol/m³).

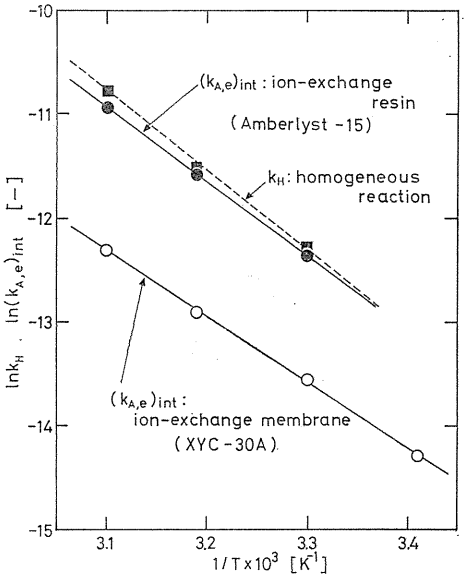

Fig. 4. 4. Arrhenius plot of $(k_{A,e})_{int}$ and k_H.

4. 3. 2. Heterogeneous reaction

When ion-exchange resins in the H^+ form are used as catalysts, the heterogeneous reaction takes place on the resin phase together with the homogeneous reaction in the liquid phase.

$$-dC_A/dt = k_{A,e}W(1-\omega)QC_A/V_i + \sqrt{k_H C_R}\cdot C_A \tag{4.4}$$

where V_i is the reaction volume at the period from t_{i-1} to t_i.

Rotating speeds were changed from 5 to 12 rps. When the speeds were higher than 8 rps, the reaction rate became constant and the interphase mass transfer resistances were negligible. The rotating speed was fixed at 10 rps for following experiments.

Also, the resistances could be estimated from published correlations, such as Levins and Glastonbury[44] for stirred

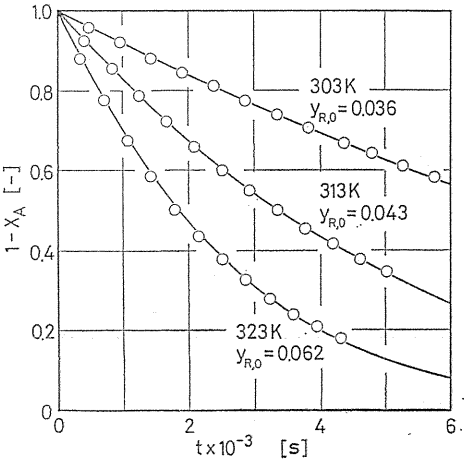

Fig. 4. 5. Conversion changes with time for the catalytic reaction in the rotating catalytic basket reactor (Catalyst: resin pellet, D_p=5.8 mm, d_p=0.095mm, W=8.07g, C_t=321mol/m³).

tank reactors and Teshima and Ohashi[45] for rotating catalytic basket reactors. The results confirmed negligible resistances.

Figure 4. 5 shows the relation of $(1-X_A)$ and t for resin pellets in the rotating catalytic basket reactor. The value of $(k_{A,e})_{obs}$ could be determined from the method of curve fitting by using Eq. (4. 4). The solid lines in Fig. 4. 5 indicate the best-fitted curves.

4. 4. *Discussion*

Figures 4. 6 and 4. 7 show the plots of $(k_{A,e})_{obs}$ vs. D_p (or d_p) at 30 and 40℃, respectively.

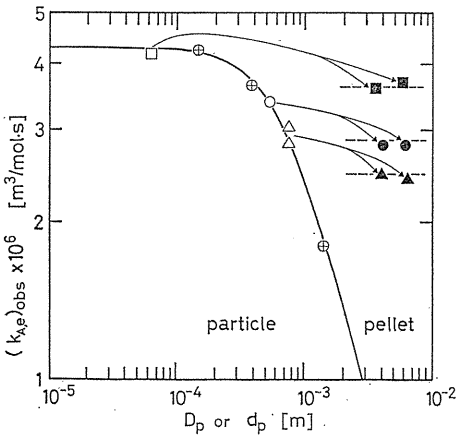

Fig. 4. 6. Influence of diameter on the rate constant at 30℃.

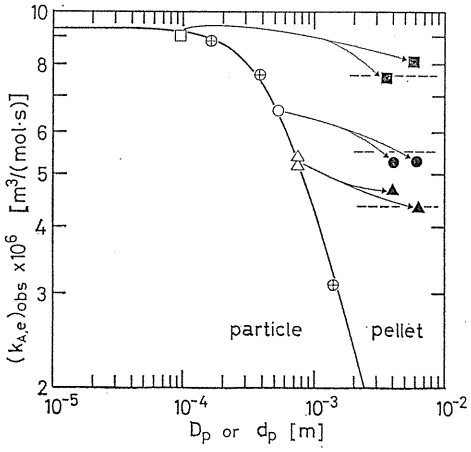

Fig. 4. 7. Influence of diameter on the rate constant at 40℃.

For resin particles, the intraparticle diffusion resistance can be evaluated by the same procedure as Section 1. 5. 1. When the ratio, $\bar{K}_A\bar{D}_A/D_{A,m}$ was equal to 0. 125, the intrinsic rate constant, $(k_{A,e})_{int}$ might be independent of the sizes of particles. The molecular diffusivity, $D_{A,m}$ could be estimated by wilke and Chang's equation as will be indicated in Table 6. 1. The Arrhenius plots of $(k_{A,e})_{int}$ for this resin are shown in Fig. 4. 4 and the activation energy (58. 6kJ/mol) was obtained from the slope.

The solid lines in Figs. 4. 6 and 4. 7 show the calculated results of $(k_{A,e})_{obs}$, which are in good agreements with the experimental values.

The value of $(k_{A,e})_{int}$ for the heterogeneous reaction are little lower than those of k_H for the homogeneous reaction. This tendency is the same as in the cases of ethyl acetate (Section 1. 5. 2) and diethyl succinate (Section 2. 4. 1).

For resin pellets, the values, the values of $(k_{A,e})_{obs}$ in Figs. 4. 6 and 4. 7 are much higher than solid lines, that is, the values calculated from the conventional method by using the effectiveness factor, Eq. (1. 24). As the diameters of constituent resins, d_p increased, the values of $(k_{A,e})_{obs}$ for the pellets were decreased. However, the values of $(k_{A,e})_{obs}$ were independent of the diameters of pellets, D_p.

The ratios of rate constants for pellets, $(k_{A,e})_{obs,pellet}$ to those for particles, $(k_{A,e})_{obs,particle}$ were plotted against the diameters of constituent resins in Fig. 4.

8. The ratio was independent of d_p and was determined as

$$(k_{A,e})_{\text{obs, pellet}}/(k_{A,e})_{\text{obs, particle}}=0.84 \tag{4.5}$$

The blocking effect of binding powder in the surface of constituent resins may cause that the ratio is less than unity. Since the size of the void between constituent resins is the same order as the diameter, the liquid in the pellet can easily go through the void and the resistance of mass transfer between constituent resins may be negligible.

The dotted lines in Figs. 4. 6 and 4. 7 are the values calculated from Eq. (4. 5).

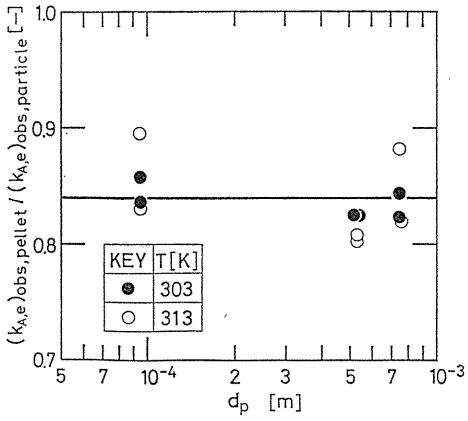

Fig. 4. 8. Ratio of $(k_{A,e})_{\text{obs, pellet}}$ to $(k_{A,e})_{\text{obs, particle}}$ vs. particle diameter.

5. Hydrolysis of Diethyl Succinate in a Recycle Reactor[15, 46]

5. 1. Introduction

A recycle reactor where a fresh feed is mixed with a portion of product stream from a tubular reactors has some advantages over reactors for experimental use. The reactor temperature can be controlled accurately. High recircuration rates permit high velocities past catalyst particles without the use of excessive reactants and the interphase mass transfer resistances can be reduced significantly. Rate data can be obtained at various conversions in one run by changing the recycle ratio. There also some disadvantages. Additional equipment such as a pump, a rotameter, and a mixing tank are required. When operating conditions are changed, the transient period may be long.

In this chapter, experimental and theoretical unsteady state data with a consecutive reaction are presented for a plug flow reactor with a mixing tank and a recycle line. Both realistic and simplified models are developed to simulate transient behavior of the recycle system. The consecutive reaction chosen for the experimental study was hydrolysis of diethyl succinate through monoethyl succinate to succinic acid on strong acid ion-exchange resin at 50℃.

5. 2. Theory

5. 2. 1. Relaistic model

Let us consider a recycle reactor system containing a plug flow reactor (V_r), a mixing tank (V_m) and a recycle line with a pump and a rotameter (V_p) as shown in Fig. 5. 1.

Step responses are given from mass balance equation as follows. The consecu-

tive reaction of first order expressed by Eq. (1. 3) takes place in the pulg flow reactor packed with catalyst particles.

Transient concentration of A and R at the outlet of the reactor are divided into two periods according to the residence time, $t_r=\varepsilon_B V_r/\{(1+\alpha)v_0\}$.

(a) When the elapsed time is shorter than the residence time $(0<t<t_r)$, the transient concentrations at the outlet are similar to those in a batch reactor.

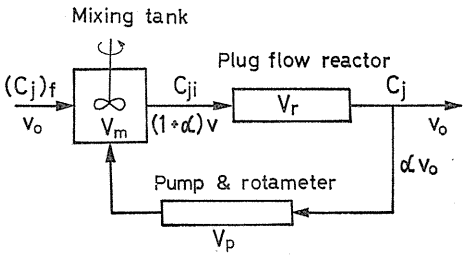

Fig. 5. 1. Realistic model of recycle reactor system.

$$C_A(t)=(C_A)_f\exp\{-k_{A,v}t(1-\varepsilon_B)/\varepsilon_B\} \tag{5.1}$$

$$C_R(t)=(C_A)_f k_{A,v}[\exp\{-k_{,Av}t(1-\varepsilon_B)/_B\} -\exp\{-k_{R,v}t(1-\varepsilon_B)/\varepsilon_B\}]/(k_{R,v}-k_{A,v}) -(C_R)_f\exp\{-k_{R,v}t(1-\varepsilon_B)/\varepsilon_B\} \tag{5.2}$$

(b) When the elapsed time is longer than the residence time $(t>t_r)$, the transientcon centrations of A and R at the outlet are

$$C_A(t)=C_{Ai}(t-t_r)\cdot f_1 \tag{5.3}$$

$$C_R(t)=C_{Ai}(t-t_r)\cdot k_{A,v}\cdot(f_1-f_2)/(k_{R,v}-k_{A,v})+C_{Ri}(t-t_r)\cdot f_2 \tag{5.4}$$

where

$$f_1=\exp\{-k_{A,v}\tau_r(1-\varepsilon_B)/(1+\alpha)\} \tag{5.5}$$

$$f_2=\exp\{-k_{R,v}\tau_r(1-\varepsilon_B)/(1+\alpha)\} \tag{5.6}$$

If the fluid in the recycle line is assumed to be in plug flow, the time lag must be taken into consideration by

$$C_{jp}(t)=C_j(t-\tau_p/\alpha)\ ;\ j=\text{A or R} \tag{5.7}$$

The mass balances around the mixing tank yield

$$C_{jo}+\alpha C_{jp}(t)-(1+\alpha)C_{ji}(t)=\tau_m dC_{ji}(t)/dt\ ;\ j=\text{A or R} \tag{5.8}$$

When the initial concentrations of A and R are identical to the feed concentrations, we have

$$C_j(0)=C_{ji}(0)=C_{jp}(0)=(C_j)_f\ ;\ \text{j=A or R} \tag{5.9}$$

Although the model described above is realistic as the representation of a recycle reactor system, Eqs. (5. 3) ~ (5. 8) cannot be solved analytially because time lags are included. A computer is required to obtain transient concentrations of A and R.

5. 2. 2. Simplified model

The realistic model may be simplified to obtain analytical solutions. Since the reactor volume (V_r) is usually much smaller than that of the mixing tank (V_m), the time lag in the reactor, t_r, may be negligible. Also, the volume of the recycle line is assumed to be included in the mixing tank. Therefore, there is no time lag in the recycle line but the volume of the mixing tank becomes (V_m+V_p) by incorporating the volumes of the pump and the rotameter in Fig. 5. 1. Substitution of Eqs. (5. 3) and (5. 4) with $t_r=0$ into Equation (5. 8) with τ_{mp} instead of τ_m and integration on the resultant equation with initial conditions of Eq. (5. 9) yields

$$C_A(t)=(C_A)_f\{f_1+(1+\alpha)(1-f_1)\exp(-g_1t)\}/(g_1\tau_{mp}) \tag{5. 10}$$

and

$$\begin{aligned} C_R(t)=&(C_A)_f f_3[\{1-\exp(-g_2t)\}/g_2 \\ &+\alpha(1-f_1)\{\exp(-g_2t)-\exp(-g_1t)\}/(g_1-g_2)] \\ &+(C_R)_f[f_2\{(1-\exp(-g_2t)\}/\tau_{mp} \\ &+g_2\exp(-g_2t)]/g_2 \end{aligned} \tag{5. 11}$$

where

$$f_3=(1+\alpha)(f_1-f_2)/[\tau_{mp}\{f_1+(1+\alpha)(1-f_1)\}(k_2/k_1-1)] \tag{5. 12}$$

$$g_1=\{f_1+(1+\alpha)(1-f_1)\}/\tau_{mp} \tag{5. 13}$$

$$g_2=\{f_2+(1+\alpha)(1-f_2)\}/\tau_{mp} \tag{5. 14}$$

5. 3. Experimental apparatus and procedure

Figure 5. 2 is a schematic drawing of the experimental apparatus. The reactor (5) was a glass tube with 3. 6cm i. d. and 10. 0cm height and the volume of reactor, V_r, was 1.02×10^{-4}m^3. The volume of the recycle line with the rotameter (7) and the circulating pump (8), V_p, was 2.32×10^{-4}m^3. The mixing tank (9) with volume, $V_m=3.88\times10^{-4}$m^3 was well mixed by a stirrer and was immersed in the water-bath (3) at 50℃. Further, all parts were maintained in the air-bath (10) at the same temperature.

At first, every part except the reactor was filled with an aqueous solution of diethyl succinate of $(C_A)_f=100$mol/m^3. Next the reactor was quickly filled with the same solution through the line (1) and then the hydrolysis of diethyl succinate occurred. The feed line was switched from line (1) to line (2) and the discharge line was opened through the flow regulator (6). The feed flow rate, v_0, was varied from 1.38×10^{-7} to 1.45×10^{-6}m^3/s and recycle ratio, α, from 1 to 24. The initial and feed concentrations of monoethyl succinate were always zero, that is, $(C_R)_f=0$mol/m^3.

The liquid sample was taken periodically from the discharge line. The concentrations of diethyl succinate (A), monoethyl succinate (R) and succinic acid (S) were determined by a liquid chromatograph (Shimazu-Du Pont, Model LC-1) with 25cm column packed with Zorbax ODS at 40℃. Aqueous methanol solution of 30%

was used as a mobile phase. The ultraviolet detector was set at a wavelength of 195nm.

A strong acid ion exchange resin, Amberlite IR-118, was used as the catalyst. The swollen resin of H^+ form was sieved in distilled water and the fraction of particles from 20 to 24 mesh (average diameter 0.78mm) was selected for use. The measured value of void fraction in the packed bed, ε_B, was 0.370.

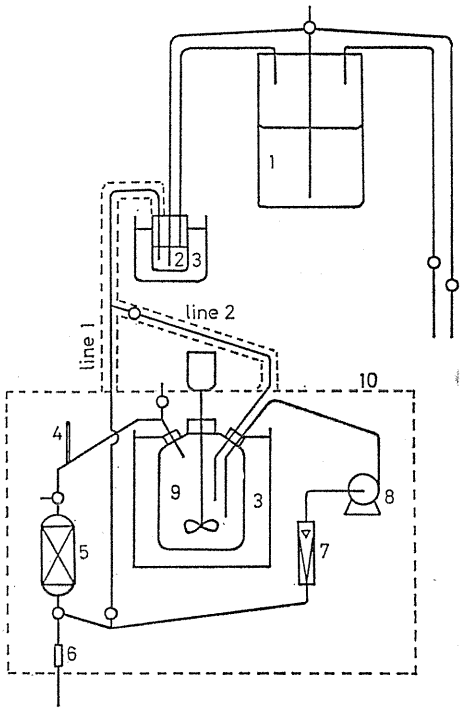

Fig. 5. 2. Schematic diagram of experimental apparatus:
① Reservoir; ② Constant head tank; ③ Water-bath; ④ Thermometer; ⑤ Reactor; ⑥ Outlet flow regulator; ⑦ Rotameter; ⑧ Circulating pump; ⑨Mixing tank; ⑩ Air-bath.

5. 4. *Results*

5. 4. 1. *Reaction rate constants from batch reactor*

To determine reaction rate constants, the consecutive reaction was studied in a glass flask batch reactor, which was immersed in a water-bath at 50℃. The stirrer was rotated at 13 rps to obtain uniform suspension of resin particles.

The experimental results are shown in Fig. 5. 3. Rate constants of first order determined by curve fitting as

$$(k_{A,v})_{obs}=1.93\times10^{-3}\mathrm{m^3\text{-solution}/(s\cdot m^3\text{-swollen resin})}$$

$$(k_{R,v})_{obs}=5.19\times10^{-4}\mathrm{m^3\text{-solution}/(s\cdot m^3\text{-swollen resin})}$$

The solid lines indicate the results calculated by using the above values of $(k_{A,v})_{obs}$ and $(k_{R,v})_{obs}$. The experimental results could be represented well by the

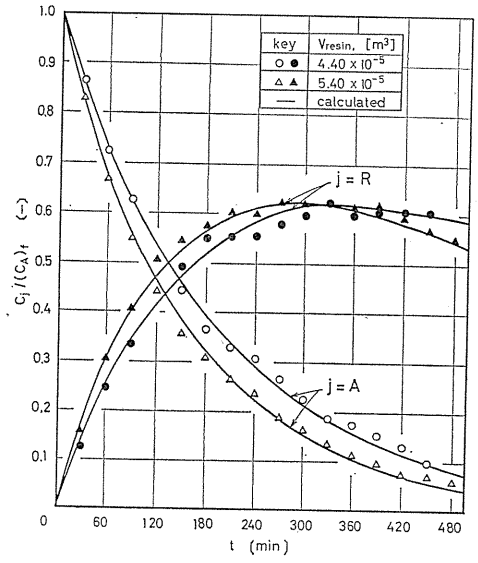

Fig. 5. 3. Hydrolysis of diethyl succinate in a batch reactor at 50℃.: $V_r=1.0\times10^{-3}\mathrm{m^3}$, $(C_A)_f=100\mathrm{mol/m^3}$, $(C_R)_f=0\mathrm{mol/m^3}$.

consecutive reaction with first order for $V_{resin}=4.40\times10^{-5}$ and $5.40\times10^{-5}m^3$-swollen resin. The values of $(k_{A,v})_{obs}$ and $(k_{R,v})_{obs}$ were used for calculations of transient responses in the following section.

5. 4. 2. Transient responses of recycle reactor

Typical experimental responses for $\alpha=2.71$, $v_0=6.03\times10^{-7}m^3/s$ are shown in Fig. 5. 4 together with two theoretical responses for the realistic and simplified models. For the realistic model, Eqs. (5. 1) ~ (5. 9) were solved numerically by Runge-Kutta-Gill method with time delay. The concentrations of A and R change rapidly until the residence time, t_r, in the reactor, i. e., 0. 3 min and then remains constant during the time lag in the recycle line, $\tau_p/\alpha=2.4$ min. After that, they gradually approach the steady-state values, $(C_A)_\infty/(C_A)_f=0.808$, $(C_R)_\infty/(C_A)_f=0.182$. For the simplified model, the concentrations of A and R were obtained from Eqs. (5. 10) and (5. 11). They change monotonously and approach to the same steady-state values as those for the realistic model. The difference between two models is small, except in the early stages of the responses. Although the experimental results have some scatter, they may be simulated by either of two models. The simplified models may be more useful than the realistic model because analytical solutions (Eqs. (5. 10) and (5. 11)) are available.

Similar results were obtained for an experiment in which $\alpha=23.6$ and $v_0=1.38\times10^{-7}m^3/s$.

5. 5. Approach time to the steady state

It is important for analysis of kinetic data to know when steady state is attained in the recycle system. Let us denote the time as $t_{i,q}$ when the concentration of i reaches $q\%$ of the steady state value. For the simplified model and the

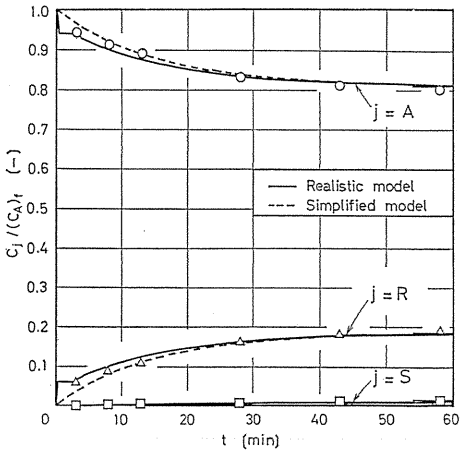

Fig. 5. 4. Transient concentration in the reactor for $\alpha=2.71$, $v_0=6.03\times10^{-7}m^3$, $V_r=1.14\times10^{-4}m^3$, $V_m=3.88\times10^{-4}m^3$, $V_p=2.32\times10^{-4}m^3$.

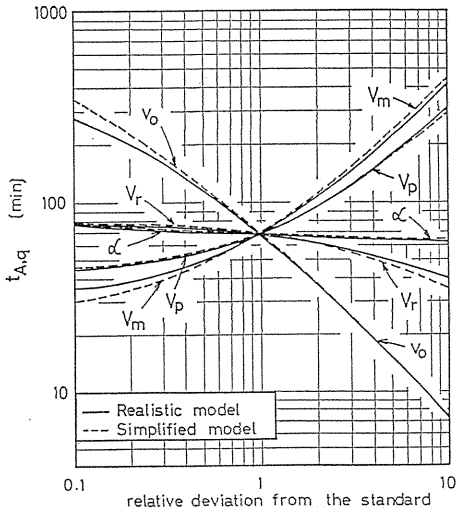

Fig. 5. 5. The relative dependence of each parameter on $t_{A,q}$ at $q=99\%$.

reactant A, the analytical solution can be obtained from Eq. (5. 10)

$$t_{A,q}=(1/g_1)\ln[(1+\alpha)(1-f_1)/\{(\tau_{mp}g_1-f_1)(1-q/100)\}] \qquad (5.15)$$

For other cases, numerical computations are required.

Fig. 5. 5 shows the relative dependence of each parameter, V_m, V_p, V_r, and v_0, on the time, $t_{A,q}$, for two models at $q=99\%$, The values in Fig. 5. 5 were chosen as the standard and each parameter was varied from 0.1 to 10 times of the standard value while the remaining parameters were fixed. It is evident from Fig. 5. 5 that the values of V_m and V_p should be decreased and the values of V_r and v_0 increased to reach the steady state as soon as possible. The difference between the realistic and simplified model results for $t_{A,q}$ is not significant. Also, the time, $t_{R,q}$, for the intermediate product R, is almost the same as that for reactant, A. Therefore, the approach time to the steady state can be approximated by the analytical solution, Eq. (5. 15).

6. Hydrolysis of Ethyl Formate in a Tube-Wall Reactor[14]

6. 1. Introduction

Tube-wall reactors, in which reactions are catalyzed at the tube wall, have certain advantages over other types of reactors such as packed beds. In the first place, temperature control is simpler, as the heat of reaction is evolved only at the wall of the tube, and in the second place, the lower pressure drop due to the absence of any packing material and the easier control of the state of flow make for a simpler mathematical treatment. Tube-wall reactors are of two types; those in which a single empty tube is used, and those which consist of two concentric tubes with different diameters.

In this chapter, a single tube-wall reactor and an annular tube-wall reactor containing ion-exchange membrans are used to study hydrolysis of ethyl formate in dilute aqueous solution. The average concentration and the radial concentration distribution at the reactor outlet will be measured and the results are compared with the theoretical predictions assuming plug flow and laminar flow.

6. 2. Experimentals

6. 2. 1. Experimental method

The plow-type reactor is shown schematically in Fig. 6. 1. The 0.2 N aqueous solution of ethyl formate flowed into the reactor inlet from the feed reservoir (1) by way of the pump (2), the flow-rate control valve (3), the rotameter (4), and the preheater (7). After reacting on part of the ion-exchange membrane which was coated on the inner wall of the outer tube, the liquid overflowed from the reactor outlet. The reactor consisted of two concentric tubes. The length of the glass outer tube was 1.1 m and its internal diameter was 2.6 cm, while the external diameter of the inner tube was either 0.6 or 1.5 cm. Some experiments were also performed without the inner tube. The length of the ion-exchange membrane was either 30 or 60 cm. The entrance region of the reactor inlet was at least 40 cm. The reaction temperature was 20, 30, 40 or 50℃.

The average conversion at the reactor outlet was determined from a sample of

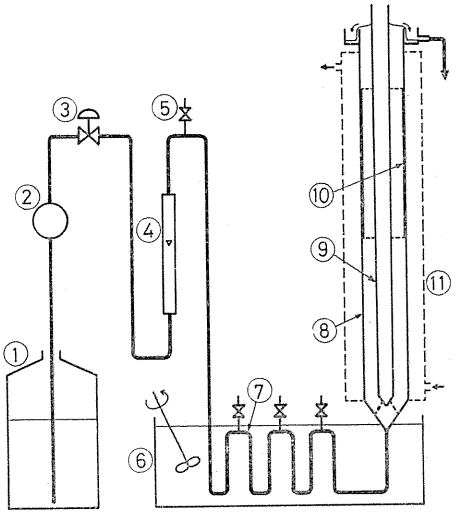

Fig. 6. 1. Experimental apparatus:
① Feed reservoir; ② Pump;
③ Valve; ④ Rotameter;
⑤ Bubble remover;
⑥ Thermostat;
⑦ Preheater; ⑧ External tube; ⑨ Internal tube;
⑩ Ion-exchange membrane;
⑪ Jacket.

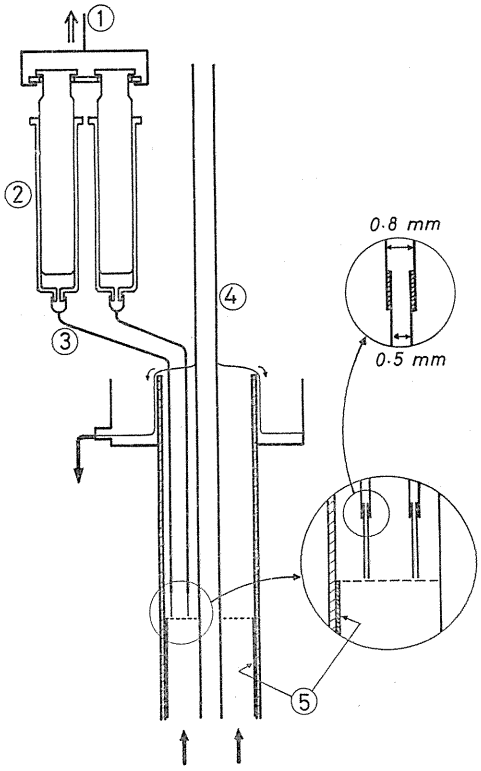

Fig. 6. 2. Details of sampling method for radial profiles of concentration:
① Microfeeder; ② Syringe;
③ Needle; ④ Internal tube;
⑤ Ion-exchanger membrane.

$5.0\times10^{-6}m^3$ of the overflow liquid. Figure 6. 2 shows the sampling method for measuring the radial concentration distribution. The tips of two syringe needles were inserted into the reactor at the same height but at different radial positions, and by rotating the motor of a microfeeder backwards, samples were withdrawn into the syringes. Since the syringe needles needed to be about 30 cm long, to ensure that they were strong enough and resistant to suction, the tips of the needles were 0. 5 mm in internal diameter, while their upper portions were 0. 8 mm in internal diameter (see the enlargement in Fig. 6. 2).

The concentration of ethyl formate was determined by the same method as in the section 4. 2. 2.

6. 2. 2. Catalysts

The tube-wall catalyst was XYC-30A cation-exchange membrane manufactured by Mitsubishi Yuka Engineering Co. It was used in the form of a smooth surface film of thickness 0. 35 mm, which was attached to the inner wall of the reactor

due to its intrinsic elasticity. Before the reactor was used, it was rinsed quickly with 10 times its ion-exchange capacity of 1 N HCl to put the catalyst into the H^+ form. The ion-exchange membrane was then washed with distilled water until no more chloride ions were present, as indicated by more milkiness with silver nitrate. The total capacity of ion-exchange per the unit surface area, Q_s was 0.674mol/m^2.

6. 3. Theory

Our intention is to compare our experimental results on hydrolysis of ethyl formate with a numerical analysis based on a model of molecular diffusion in the bulk liquid phase and chemical reaction at the tube wall.

Let us assume that the reaction is a first-order reaction which is taking place only on the inner wall of the outer cylinder of the annular tube. If we assume that longitudinal dispersion is negligible, the mass barance equation will be

$$u(r)\partial C_A/\partial l = D_{A,m}\{\partial^2 C_A/\partial r^2 + (2/r)\partial C_A/\partial r\} \tag{6.1}$$

which can be put into dimensionless form on the basis of the dimensionless terms listed under Nomenclature;

$$p(x)\partial z/\partial y = \partial^2 z/\partial x^2 + (1/x)\partial z/\partial x \tag{6.2}$$

where $p(x)$ is the dimensionless radial velocity profile, fo plug flow,

$$p(x) = 1 \tag{6.3}$$

and for laminar flow;

$$p(x) = 2\{1 - x^2 - (1-K^2)\ln x/\ln K\}/\{1 + K^2 + (1-K^2)/\ln K\} \tag{6.4}$$

K is the ratio of the external radius of the inner tube to the internal radius of the external tube. When there is no inner tube, $K=0$, and Eq. (6. 4) simplifies to

$$p(x) = 2(1-x^2) \tag{6.5}$$

The boundary conditions are

$$\text{when } y=0,\ z=1 \tag{6.6}$$

$$\text{when } x=0,\ \partial z/\partial x = -Da \tag{6.7}$$

$$\text{when } x=K,\ \partial z/\partial x = 0 \tag{6.8}$$

The average, cross-sectional dimensionless concentration z is defined as

$$z = \{2/(1-K^2)\}\int_K^1 x p(x) z \mathrm{d}x \tag{6.9}$$

The above equation has been used as the basis of an analytical solution for the case of plug flow in a single tube without any inner tube (equivalent to $K=0$ and $p(x)=1$).[47] The average concentration is given by the expression

$$z = \sum_{n=1}^{\infty}[4\exp(-\beta_n^2 y)/\{\beta_n^2(1+\beta_n^2/Da)\}] \tag{6.10}$$

where the eigen value β_n is the n-th root of the equation

$$\beta_n J_1(\beta_n)/J_0(\beta_n)=Da \tag{6.11}$$

For the case of laminar flow in a single tube without an inner tube, Brauer et al.[48] solved Eq. (6. 2) by the method of separation of variables and obtained a numerical solution by a method in which a coefficient was derived from the infinitesimal change in the eigen value. Shitaokoshi[49] extended the method of Brauer et al.[48] to obtain a general method of calculation which can also be used in the case of an annular tube. Some calculated data for the average outlet concentration and the radial concentration profile which were obtained by electronic computer using this method have been plotted in Fig. 6. 3~6. 7 to form a basis of comparison with our own experimental results.

6. 4. Results and discussion

6. 4. 1. Reaction rate constant as determined in a recirculating-type of batch reactor

In order to determine the true reaction rate in the absence of mass transfer, the flow-type of experimental apparatus shown in Fig. 6. 1 was altered into a recirculating-type batch reactor. Only the pump, the rotameter and the empty tube reactor with the constant-temperature jacket were used to circulate the liquid rapidly. A quantity of $8.35\times10^{-4}m^3$ of distilled water was circulated through the reactor until its temperature was constant. Then, $1.5\times10^{-5}m^3$ of ethyl formate was introduced into the reactor so that its initial concentration was 0. 2N. Taking this point of time as the reaction initiation time, $5.0\times10^{-6}m^3$ samples were taken at the outlet of the reactor at fixed time intervals, and the concentration of formaic acid which was formed determined by neutralization titration.

In order to determine the mass-transfer resistance in the bulk liquid, experiments were conducted at different average velocities in the reactor over the range 0. 1~0. 7m/s. It was found that $k_{A,e}$ did not vary, even though the velocity of flow was varied, so that this was true reaction rate constant in the absence of mass transfer.

Figure 4. 4 is the Arrhenius plot of the rate constant, $k_{A,e}$ at temperatures of 20, 30, 40, and 50℃. The graph was linear, its slope being the activation energy 50. 2kJ/mol. The rate constant of ion-exchange membrane, XYC-30A is less by about 0. 28 times than that of ion-exchange resin, Amberlyst 15. Table 6. 1 gives the values of the reaction rate constant $k_{A,e}$, the molecular diffusivity $D_{A,m}$, and the Damköhler number, Da.

Table 6. 1. The values of $k_{A,e}$, $D_{A,m}$ and Da.

Temperature [℃]	$k_{A,e}\times10^6$ [m³/(mol·s)]	$D_{A,m}\times10^9$ [m²/s]	Da [−]
20	0.638	1.04	5.25
30	1.31	1.34	8.30
40	2.49	1.70	12.5
50	4.51	2.09	18.4

6. 4. 2. Average concentration at the outlet of the tube-wall catalytic reactor

The empirical unconverted fraction as determined at 30℃ in the annular reactor ($K=0.593$) and the theoretical values for plug and laminar flow are plotted versus axial coordinate y as shown in Fig. 6. 3. In order to show the edge effect due to differences in the length of the ion-exchange membrane, the empirical data for $L=0.3$ and 0. 6m have been plotted on the graph. However, the differences were within the range of experimental error, and so no edge effect could be confirmed.

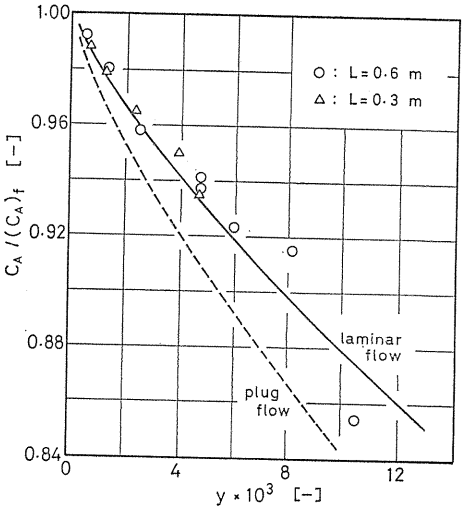

Fig. 6. 3. Average exit concentrations at $K=0.593$ and 30℃.

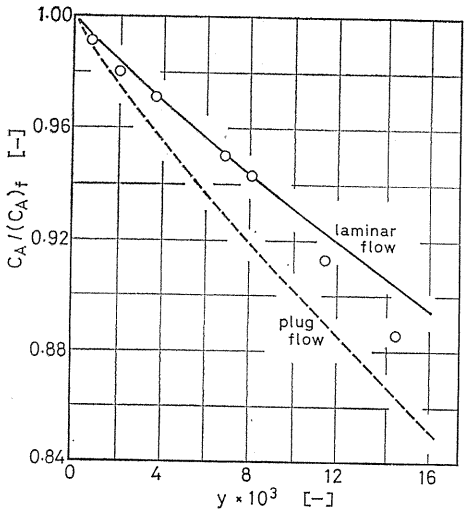

Fig. 6. 4. Average exit concentrations at $K=0.237$, $L=0.6$m and 30℃.

The empirical data agreed closely with the theoretical data for laminar flow.

Figure 6. 4 shows the corresponding results for a lower ratio between the external diameter of the inner tube and the internal diameter of the outer tube, namely $K=0.237$. Although the empirical data were in good afreement with the theoretical data for laminar flow, there was a slight divergence between the two as the dimensionless axial coordinate y increased. This would seem to be due to the effect of turbulence at lower values of K, which means that the space between the annular tubes was increased. When $K=0$, that is, in a single-tube reactor, as Fig. 6. 5 shows, the empirical data lay somewhere between the theoretical data

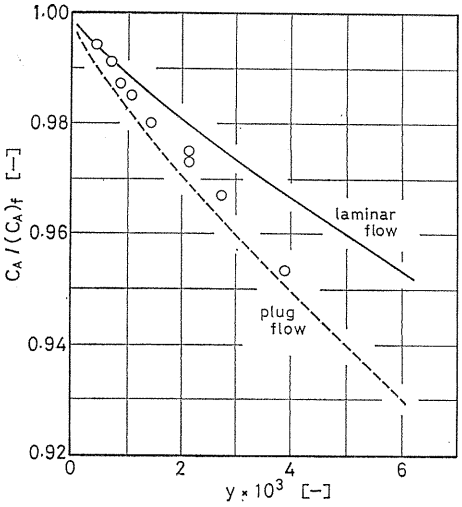

Fig. 6. 5. Average exit concentrations at $K=0$, $L=0.6$m and 30℃.

for plug flow and laminar flow, which is quite different from the behavior with the annular reactor.

6. 4. 3. Radial concentration distribution in the tube-wall catalytic reactor

Figure 6. 6 shows the empirrical results for the annular reactor with $K=0.237$. The solid line represents the radial concentration distribution as calculated on the basis of laminar flow, where the velocity distribution was as shown by the dotted line. The very close agreement between the theoretical and the empirical results is evident. Even when the average velocity was varied over the range $(1\sim 2)\times 10^{-3}$m/s, there was no change in the concentration distribution. Although there was a sudden decrease in the concentration as the dimensionless radial coordinate went from 0. 8 to 1 (the actual distance was about 2. 5mm), it is surprising that there was no disturbance in the flow when the samples were taken.

In the case of the single-tube reactor, Fig. 6. 7 shows that the empirical concentration distribution differed considerably from the theoretical distribution, assuming laminar flow, for which the velocity distribution was as represented by the dotted line, this indicating the strong effect of radial turbulent mixing.

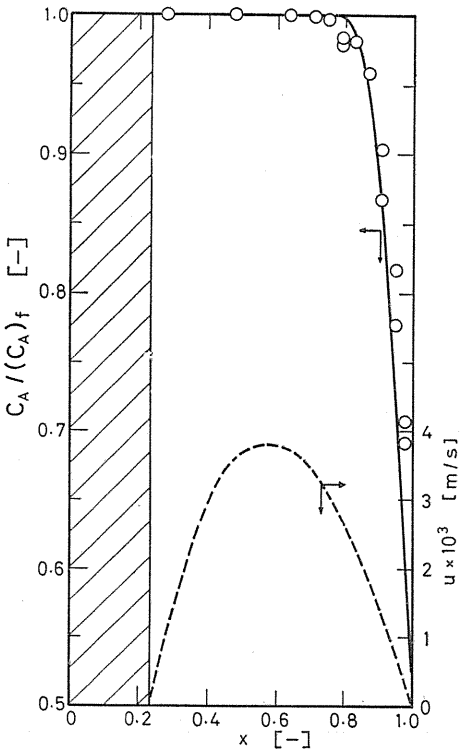

Fig. 6. 6. Radial porfile of concentrations at $K=0.237$, $y=2.01\times 10^{-3}$, $L=0.6$m and 30℃.

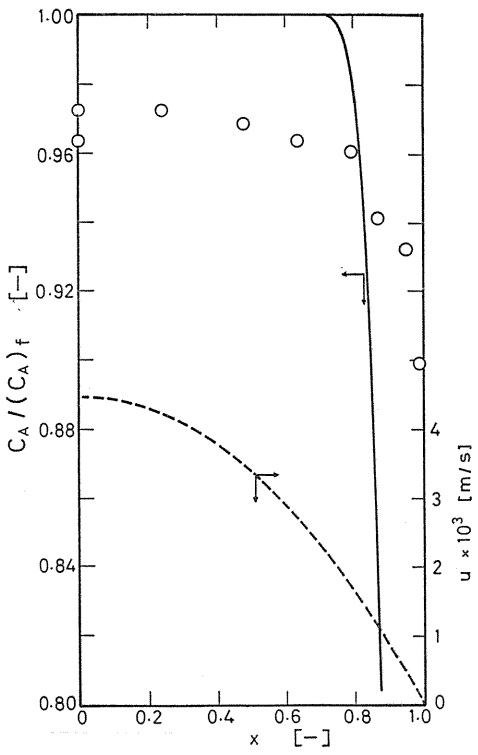

Fig. 6. 7. Radial profile of concentrations at $K=0$, $y=2.71\times 10^{-3}$, $L=0.6$m and 40℃.

7. Evaluations of Mass Transfer Resistances by Using Ion-Exchange Resins

7. 1. Evaluation of intraparticle diffusivity[34]

The intraparticle diffusivity of sodium and hydrogen ions in the cation-exchange resin, Amberlite IR-120L (the average diameter =0.929mm) were studied by using a recycle reactor. A method of analysis was developed for the diffusion controlled ion-exchange velocity in the particle at non-zero concentration of eluting ion at its surface.

The self-diffusion coefficient of sodium ion was evaluated from the interdiffusion coefficient by applying the approximation developed by Helfferich and Plesset[50] and applied by Rao and David[51]. The results showed a good coincidence with that obtained by the use of the isotopes. The diffusivity decreased with the increase in exchange time. This may be attributed to time lag in the measurement, the microheterogeneity of particles and the water content in resin pores at the beginning of the measurement.

7. 2. Simultaneous evaluations of mass transfer resistances[52, 53]

A method ef simultaneous evaluations of the interphase mass transfer coefficient and the intraparticle diffusivity from batchwise ion-exchange rate data was proposed. An apparent mass transfer coefficient which was determined by neglecting intraparticle diffusion resistances could be used to evaluate the individual coefficients. If the values of the apparent mass transfer coefficient are independent of time, the intraparticle diffusion resistance may be negligible. On the other hand, if the values of apparent coefficient decrease with time, the resistance may be significant and the degree of the dacrease presents the magnitude of the intraparticle diffusion resistance.

For the case of linear isotherm, published data of Huang and Li[54] were used for isotopic ion-exchange data between calcium chloride solutions and a calcium form cation-exchange resin, Dowex 50W-X8. For the case of nonlinear isotherms, the rates of exchange of H^+ and Na^+ ions with a strong acid ion-exchange resin, Dowex 50W-X12 were measured in a batchwise stirred tank. The values evaluated from this method were in good agreement with those estimated from published correlations.

7. 3. Liquid-solid mass transfer in gas-liquid cocurrent packed beds[55]

Rates of mass transfer from liquid phase to small particles (average diamer =0.46~1.3mm) were measured by use ef ion-exchange reaction followed by instantaneous irreversible reaction at 30℃. Nitrogen gas and dilute aqueous solution of NaOH were fed into a shallow bed packed with a strong cation-exchange resin, Amberlyst 15. Volumetric mass transfer coefficients for gas-liquid cocurrent upflow and downflow were almost identical at the same gas and liquid flow rates but become somewhat grater than those in liquid-full single phase flow. The unified correlation could be derived by arranging experimental data for three arrangements: liquid-full single phase flow, gas-liquid cocurrent upflow and downflow.

This correlation was based on the enhancement factor and Dwivedi and Upa-

dhyay's correlation[56] for single phase flow.

7. 4. Liquid-solid mass transfer in basket type three-phase reactors[57]

Basket type stirred tank reactors may be useful for three phase reactions, that is, reactions between dissolved gas and liquid on solid catalysts because there is no fear of sedimentations of catalyst particles to the bottom even if large, heavy particles are used.

Rates of mass transfer from liquid to solid in bastet type reactors were measured for liquid-solid system by Suzuki and Kawazoe[58] and Teshima and Ohashi.[45] The mass transfer coefficients were greater than those in a stirred slurry reactor. On the other hand, when gas was introduced, Pavko et al.[59] found that the apparent rate constants in basket type reactors were less than those in the liquid-full reactor and that the inactivity of the catalyst might be due to the gas bubbles entrapped inside catalyst baskets. Also, if the screen openings are very narrow, it may be difficult for the liquid to go through the baskets and mass transfer coefficients become smaller.

To check the effects of gas flow rates, screen openings and locations of bakets on mass transfer coefficients, rates of mass transfer from liquid to solid were measured in batch reactors by using ion exchange reaction between the resin in the H^+ form and sodium hydroxide. Mass transfer coefficients in three types of reactors were compared with published correlations.[44, 55, 60]

Nomenclature

a_i	=parameter defined by Eq. (3. 26)	[—]
b_i	=parameter defined by Eq. (3. 27)	[—]
$(C_A)_f$	=feed concentration of A in the organic phase $(=(m_A)_f/V_{org})$	[mol/m^3]
$C_{i,j}$	=concentration in the liquid phase (j=org or aq)	[mol/m^3]
$\bar{C}_i$	=concentration in the resin phase	[mol/m^3]
$D_{i,m}$	=molecular diffusivity	[m^2/s]
$\bar{D}_i$	=effective diffusivity of resin phase	[m^2/s]
Da	=Damköhler number $(=k_{A,e}Q_s\ (d_t/2)/D_{A,m})$	[—]
D_p	=pellet diameter	[m]
d_p	=particle diameter	[m]
d_t	=inner diameter of reactor	[m]
E	=fractional apparoch to equlibrium	[—]
E_{fi}	=effectiveness factor	[—]
e	=parameter dehined by Eq. (3. 30)	[—]
H	=height of resin pellet	[m]
$J_0(\beta_n)$	=Bessel function of zero order	[—]
$J_1(\beta_n)$	=Bessel function of first order	[—]
K	=radii ratio of internal to external tube	[—]
K_H	=dissociation	[mol/m^3]
K_i	=distribution coefficient defined by Eq. (3. 5)	[—]
$\bar{K}_i$	=adsorption coefficient defined by Eq. (1. 8)	[—]
k_H	=rate constant of first order for the homogeneous reaction based on the acid concentration	[s^{-1}]
$k_{i,e}$	=rate constant of first order based on the equivalent	[m^3/(mol·s)]

$k_{i,j}$	=rate constant of first order in the liquid phase (j=org or aq)	[s^{-1}]
$k_{i,v}$	=rate constant of first order based on the volume of resin and the concentration in the liquid phase	[s^{-1}]
$\bar{k}_i$	=rate constant of first order in the resin phase	[s^{-1}]
L	=diameter of resin pellet or length of reactor	[m]
l	=axial coordinate in the reactor	[m]
$m_{i,j}$	=moles in the liquid phase (j=org or aq)	[mol]
$\bar{m}_i$	=moles in the resin phase	[mol]
$\bar{N}_i$	=mass flux in the resin phase	[mol/(m^2·s)]
$p(x)$	=dimensionless radial profile of velocity (=u(r)/$\bar{u}$)	[—]
Q	=total capacity of ion-exchange based on the mass of dry resin	[mol/kg-dry resin]
Q_s	=total capacity of ion-exchange membrane based on the surface	[mol/m^2-swollen resin]
Q_v	=total capacity of ion-exchange based on the volume of swollen resin	[mol/m^3 -swollen resin]
$R_{i,j}$	=reactionrate in the liquid phase (j=org or aq)	[mol/(m^3·s)]
$\bar{R}_i$	=reaction rate in the resin phase	[mol/(m^3·s)]
r	=radial position within particle or reactor	[m]
$u(r)$	=radial profile of velocity	[m/s]
$\bar{u}$	=average velocity	[m/s]
$S_H{}^i$	=selectivity coefficient	[—]
t	=time	[s]
V_j	=volume in the liquid phase (j=org or aq)	[m^3]
V_m	=volume of mixing tank	[m^3]
V_p	=volume of recycle line	[m^3]
V_r	=volume of reactor	[m^3]
v_0	=flow rate at the feed line	[m^3/s]
W	=weight of swollen resin	[kg-swollen resin]
X_A	=conversion of component A	[—]
x	=dimensionless radial coordinate ($=r/(d_t/2)$)	[—]
y	=dimensionless axial coordinate ($=4lD_{A,m}/(ud_t{}^2)$)	[—]
$y_{i,\mathrm{aq}}$	=dimensionless concentration of component i in the aqueous phase ($=C_{i,\mathrm{aq}}/(C_A)_f$)	[—]
$y_{i,\mathrm{org}}$	=dimensionless concentration of component i in the organic phase ($=C_{i,\mathrm{org}}/(C_A)_f$)	[—]
z_i	=dimensionless concentration of component i in the resin phase ($=\bar{C}_i/(\bar{C}_A)_f$)	[—]

Greek symbols

α	=recycle ratio	[—]
α_i	$=\bar{k}_i(d_p/2)^2/\bar{D}_A$	[—]
β_i	$=3W\bar{K}_A\delta_i/(V\rho_p)$	[—]
β_n	=eigen value	[—]
γ	$=V_{\mathrm{aq}}/V_{\mathrm{org}}$	[—]
$\bar{\gamma}$	$=(W/\rho_p)V_{\mathrm{org}}$	[—]
δ_i	$=\bar{D}_i/\bar{D}_A$	[—]
ε	$=E_{fR}/E_{fA}$	[—]
ε_B	=void fraction in the bed	[—]

ε_p'	=void fraction in the pellet	[—]
$\zeta_{i,j}$	=parameter defined by Eq. (3. 19)	[—]
$\bar{\zeta}_i$	=parameter defined by Eq. (3. 18)	[—]
θ	$=\bar{D}_A t/(d_p/2)^2$	[—]
κ	$=\bar{k}_R/\bar{k}_A$	[—]
ξ	$=r/(d_p/2)$	[—]
ρ_p	=density of swollen resin	[kg/m^3-swollen resin]
τ_m	$=V_m/v_o$	[s]
τ_{mp}	$=(V_m+V_p)/v_o$	[s]
τ_p	$=V_p/v_o$	[s]
τ_r	$=V_r/v_o$	[s]
ϕ_i	$=\bar{K}_i/\bar{K}_A$	[—]
ω	=fraction of moisture content in swollen resins	[—]

<Subscripts>

A	=reactant
aq	=aqueous phase
f	=initial state
i	=component (A, R, S)
int	=intrinsic
j	=phase (organic, aqueous or resin phase)
obs	=observed
org	=organic phase
R	=intermediate product
S	=final product
∞	=equilibrium

References

1) G. G. Thomas and C. W. Davies, "Ion Exchange Resins as Catalysts", *Nature*, **159**, 372 (1947).
2) N. L. Smith and N. R. Amundson, "Intraparticle Diffusion in Catalytic Heterogeneous Systems", *Ind. Eng. Chem.*, **43**, 2156 (1951).
3) W. H. Wadman, "Some Reactions of Sugar Catalysed by a Cation-Exchange", *J. Chem. Soc.*, 3051 (1952).
4) C. W. Davies and G. G. Thomas, "Ion-Exchang Resins as Catalysts in the Hydrolysis of Esters", *J. Chem. Soc.*, 1607 (1952).
5) S. A. Bernhiard and L. P. Hammett, "Specific Effects in Acid Catalysis by Ion Exchange Resins", *J. Amer. Chem. Soc.*, **75**, 1798 (1953), **75**, 5834 (1953), **76**, 991 (1954), **76**, 992 (1954).
6) F. Helfferich, "A Quantitative Approach to Ion Exchange Catalysis", *J. Amer. Chem. Soc.*, **76**, 5567 (1954).
7) K. Saito, F. Shimamoto, Y. Mishima and O. Sataka, "Liquid-Phase Reaction Rates on Ion-Exchange Resin Catalysts", *Kogyo Kagaku Zasshi*, **64**, 1733 (1961).
8) K. Saito, "Catalytic Effectiveness Factors of Ion-Exchange Resin Catalysts", *Kogyo Kagaku Zasshi*, **64**, 1738 (1961).
9) K. Rajamani, S. C. Shenoy, M. S. Rao and M. G. Rao, "Kinetics of the Hydrolysis of Ethyl Acetate Catalysed by Cation-Exchange Resin", *J. appl. Chem. Biotechnol.*, **28**, 699 (1978).

10) H. Teshima, T. Sumi and N. Morita, "Effects of Resin Structure on the Rate of Hydrolysis of Esters Catalyzed by Cation Exchange Resins", *Shokubai*, **13**, 13P (1971).
11) H. Teshima, T. Sumi and N. Morita, "Effects of Diffusion and Adsorption of Reactant in Resin Phase on the Rate of Hydrolysis of Esters Catalyzed by Cation Exchange Resins", *Nihon Kagakukaishi*, 7111 (1972).
12) H. Teshima, T. Sumi and N. Morita, "Effects of the Acid Contents of the Cation Exchange Resins on the Catalytic Activities", *Nihon Kagakukaishi*, 2045 (1972).
13) H. Teshima, T. Ido and T. Kasahara, "Effects of the Acid Contents and Replacing Ions of the Macroreticular Type Ion Exchange Resins on the Catalytic Activities for Hydrolysis of Ethyl Acetate", *Nihon Kagakukaishi*, 769 (1977).
14) S. Shitaokoshi, S. Goto and H. Teshima, "Hydrolysis of Ethyl Formate on Ion-Exchange Membrane in a Tube Wall Reactor", *Kagaku Kogaku Ronbunshu*, **7**, 178 (1981).
15) T. Ido, M. Goto and H. Teshima, "Transient Behavior of Recycle Reactor with Consecutive Reaction", *Can. J. Chem. Eng.*, **60**, 407 (1982).
16) S. Shitaokoshi, S. Goto and H. Teshima, "Hydrolysis of Ethyl Formate in a Tube-Wall Catalytic Reactor", *Inter. Chem. Eng.*, **23**, 503 (1983).
17) M. Goto, S. Goto and H. Teshima, "Hydrolysis of Diethyl Succinate Catalyzed by Cation Exchange Resin", *J. Chem. Eng. Japan*, **16**, 223 (1983).
18) K. Nishimura and S. Goto, "Catalytic Activities of Pellets Made of Ion-Exchange Resins", *Kagaku Kogaku Ronbunshu*, To be published.
19) H. Teshima, S. Goto, T. Ido and N. Oyama, "Kinetics and Processes of Chemical Reaction with Solid Phase Transfer Catalysts (Part 1)", *Rept. of Asahi Glass Found. for Ind. Tech.*, **39**, 59 (1981).
20) H. Teshima, S. Goto, T. Ido and H. Tariki, "Kinetics and Processes of Chemical Reaction with Solid Phase Transfer Catalysts (Part 2)", *Rept. of Asahi Glass Found. for Ind. Tech.*, **40**, 290 (1982).
21) T. Ido, N. Oyama, S. Goto and H. Teshima, "Kinetics of Oxidation of Benzyl Alcohol with Solid Phase Transfer Catalyst", *Kagaku Kogaku Ronbunshu*, **9**, 58 (1983).
22) T. Ido, N. Oyama, S. Goto and H. Teshima, "Kinetics of Oxidation of Benzyl Alcohol with a Solid Phase Transfer Catalyst", *Inter. Chem. Eng.*, To be published.
23) T. Ido, H. Tariki, K. Sakurai and S. Goto, "Intraparticle Diffusion in Solid Phase Transfer Catalyst for Oxidation of Benzyl Alcohol", *Kagaku Kogaku Ronbunshu*, To be published.
24) S. Sussman, "Catalysis by Acid-Regenerated Cation Exchangers", *Ind. Eng. Chem.*, **38**, 1228 (1946).
25) C. L. Levesque and A. M. Craig, "Kinetics of an Esterification with Cation-Exchange Resin Catalyst", *Ind. Eng. Chem.*, **40**, 96 (1948).
26) S. K. Ihm, S. S. Suh and I. H. Oh, "Reaction and Mass Transfer in a Macroreticular Resin Catalyst", *J. Chem. Eng. Japan*, **15**, 206 (1982).
27) G. E. Barker and R. R. White, "Rates of Alcoholysis and Diffusion in Ion-Exchange Resins", *Chem. Eng. Progr. Symp. Ser.*, 48 No. 4, 75 (1952).
28) Y. Murakami and O. Mori, "Sucrose Inversion on Amberlyst 15", *Kogyo Kagaku Zasshi*, **69**, 588 (1966).
29) E. R. Gilliand, H. J. Bixler and J. E. O'Connell, "Catalysis of Sucrose Inversion in Ion-Exchange Resins", *IEC Fund.*, **10**, 185 (1971).
30) M. J. Astle and J. A. Zaslowsky, "Reactions Catalyzed by Anion Exchange Resin", *Ind. Eng. Chem.*, **44**, 2867 (1952).
31) P. N. Unni and S. Bhatia, "Alkylation of Phenol with Isobutene Catalysed by Cation Exchange Resin ... a Kinetic Study", *J. Chem. Tech. Bietechnol.*, **33A**, 1 (1982).
32) C. J. Schmidle and R. C. Mansfield, "Catalysis by Anion Exchange Resins", *Ind. Eng. Chem.*, **44**, 1388 (1952).
33) F. Helfferich, "Ion Exchange", Chap. 11, pp. 519–550, McGraw-Hill, New York (1962).
34) T. Kawabe, H. Teshima and N. Morita, "Intraparticle Diffusivity of Sodium Ion in Amberlite IR-120L Ion Exchange Resin", *Kogyo Kagaku Zasshi*, **70**, 133 (1967).

35) S. Liu, "Numerical Solution of Two-Point Boundary Value Problems in Simultaneous Second-Order Nonlinear Ordinary Differenial Equations", *Chem. Eng. Sci.*, **22**, 871 (1967).
36) J. J. Barker and R. E. Treybal, "Mass Transfer Coefficients for Solids Suspended in Agitated Liquids", *AIChE Journal*, **6**, 289 (1960).
37) C. N. Satterfield, "Mass Transfer in Heterogeneous Catalysis", pp. 164-207, MIT Press, Massachusetts (1970).
38) H. S. Harned and R. Pfanstiel, "A Study of the Velocity of Hydrolysis of Ethyl Acetate", *J. Amer. Chem. Soc.*, **44**, 2193 (1922).
39) T. Kataoka, H. Yoshida and H. Sanada, "Estimation of the Resin Phase Diffusivity in Isotopic Ion Exchange", *J. Chem. Eng. Japan*, **7**, 105 (1974).
40) C. M. Starks and C. Liotta, "Phase Transfer Catalysis", Academic Press, New York (1978).
41) S. L. Regen, "Triphase Catalysis", *J. Amer. Chem. Soc.*, **97**, 5956 (1975), **98**, 6270 (1976), **101**, 4059 (1979).
42) K. Hashimoto, K. Miura and S. Nagata, "Intraparticle Diffusivities in Liquid-Phase Adsorption with Nonlinear Isotherms", *J. Chem. Eng. Japan*, **8**, 367 (1975).
43) C. H. Bamford and C. F. H. Tipper, "Ester Formation and Hydrolysis and Related Reactions", pp. 101-25, Elsevior Publishing Company, Amsterdam (1972).
44) D. M. Levins and J. R. Glastonbury, "Particle-Liquid Hydrodynamics and Mass Transfer in a Stirred Vessel", *Trans. Instn Chem. Engrs*, **50**, 132 (1972).
45) H. Teshima and Y. Ohashi, "Particle to Liquid Mass Transfer in a Rotating Catalyst Basket Reactor", *J. Chem. Eng. Japan*, **10**, 70 (1977).
46) N. Morita and H. Teshima, "Evaluation of Rate Data -Ⅱ Differential Reactor and its Alternatives", *AIChE Modular Instruction*, **2**, 59 (1981).
47) G. Damköhler, "Einflusse der Stromung. Diffusion und des Warmeuberganges auf die Leistung von Reaktionsofen", *Z. Elektrochem.*, **42**, 846 (1936).
48) H. Brauer and H. Schluter, "Konvektiver Stoffaustausch mit Heterogener Chemischer Reaktion", *Chemie Ing. Techn.*, **37**, 1107 (1965).
49) S. Shitaokoshi, "The Performance of Tube-Wall Catalytic Reactor with Ion-Exchange Membrane" Master Thrsis in Nagoya Univ. (1980).
50) F. Helfferich and M. S. Plesset, "Ion-Exchange Kinetics. A Nonlinear Diffusion Problem", *J. Chem. Phys.*, **28**, 418 (1958).
51) M. G. Rao and M. M. David, "Single-Particle Studies of Ion-Exchange in Packed Beds. Cupric Ion-Sodium Ion System", *AJChE Journal*, **10**, 213 (1964).
52) S. Goto, M. Goto and H. Teshima, "Simplified Evaluations of Mass Transfer Resistances from Batch-Wise Adsorption and Ion-Exchange Data. 1. Linear Isotherms", *IEC Fund.*, **20**, 368 (1981).
53) M. Goto, S. Goto and H. Teshima, "Simplified Evaluations of Mass Transfer Resistances from Batch-Wise Adsortion and Ion-Exchange Data. 2. Nonlinear Isotherms", *IEC Fund.*, **20**, 371 (1981).
54) T. C. Huang and K. Y. Li, "Ion-Exchange Kinetics for Calcium Radiotracer in a Batch System", *IEC Fund.*, **12**, 50 (1973).
55) M. Yoshikawa, K. Iwai, S. Goto and H. Teshima, "Liquid-Solid Mass Transfer in Gas-Liquid Cocurrent Flows through Beds of Small Packings", *J. Chem. Eng. Japan*, **14**, 444 (1981).
56) P. N. Dwivedi and S. N. Upadhyay, "Particle-Fluid Mass Transfer in Fixed and Fluidized Beds", *IEC Process Des. Devlop.*, **16**, 157 (1977).
57) S. Goto and T. Saito, "Liquid-Solid Mass Transfer in Basket Type Three-Phase Reactors", *J. Chem. Eng. Japan*, To be published.
58) M. Suzuki and K. Kawazoe, "Particle-to-Liquid Mass Transfer in a Stirred Tank with a Basket Impeller", *J. Chem. Eng. Japan*, **8**, 79 (1975).
59) A. Pavko, D. M. Misic and J. Levec, "Kinetics in Three-Phase Reactors", *Chem. Eng. J.*, **21**, 149 (1981).

60) Y. Sano, N. Yamaguchi and T. Adachi, "Mass Transfer Coefficients for Suspended Particles in Agitated Vessel and Bubble Columns", *J. Chem. Eng. Japan*, **7**, 255 (1974).